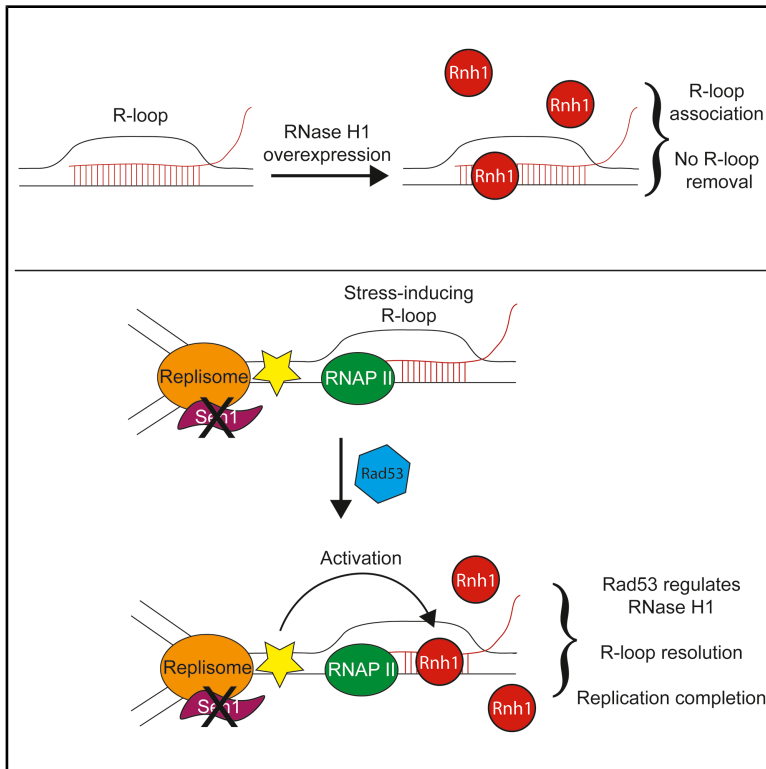


Rad53 regulates RNase H1, which promotes DNA replication through sites of transcription-replication conflict

Graphical abstract



Authors

Carolin B. Wagner, Matteo Longaretti, Sophia G. Sergi, ..., Amir Aharoni, Helle D. Ulrich, Brian Luke

Correspondence

brialuke@uni-mainz.de

In brief

Wagner et al. demonstrate that RNase H1 only removes a subset of R-loops *in vivo*. In yeast, overexpressed *RNH1* acts more frequently at dysregulated R-loops and infrequently, if at all, at other RNA-DNA hybrids. Endogenous Rnh1 is induced in a Rad53-dependent manner at transcription-replication conflicts to promote replication completion.

Highlights

- Overexpressed RNase H1 only resolves dysregulated RNA-DNA hybrids
- Endogenous RNase H1 levels increase when Sen1 function is impaired
- The Rad53 checkpoint kinase is required to increase RNase H1 levels upon Sen1 loss
- RNase H1 promotes timely replication at transcription-replication conflicts



Article

Rad53 regulates RNase H1, which promotes DNA replication through sites of transcription-replication conflict

Carolin B. Wagner,¹ Matteo Longaretti,¹ Sophia G. Sergi,¹ Neha Singh,² Ioannis Tsirkas,³ Fabio Bento,¹ Ronald P. Wong,⁴ Maya Wilkens,^{1,4} Stephan Hamperl,³ Falk Butter,^{4,5} Amir Aharoni,² Helle D. Ulrich,⁴ and Brian Luke^{1,4,6,*}

¹Institute of Developmental Biology and Neurobiology (IDN), Johannes Gutenberg Universität, 55128 Mainz, Germany

²Department of Life Sciences and the National Institute for Biotechnology in the Negev, Ben-Gurion University of the Negev, Be'er Sheva 84105, Israel

³Chromosome Dynamics and Genome Stability, Institute of Epigenetics and Stem Cells, Helmholtz Munich, 81377 Munich, Germany

⁴Institute of Molecular Biology (IMB), Ackermannweg 4, 55128 Mainz, Germany

⁵Present address: Institute of Molecular Virology and Cell Biology, Friedrich-Loeffler-Institut, Südufer 10, 17493 Greifswald, Germany

⁶Lead contact

*Correspondence: brialuke@uni-mainz.de

<https://doi.org/10.1016/j.celrep.2025.116565>

SUMMARY

RNA-DNA hybrids and R-loops can lead to extensive DNA damage and loss of genomic integrity if not regulated in a timely manner. Although RNase H1 overexpression is frequently used as a tool to resolve R-loops, the regulation of RNase H1, overexpressed or endogenous, remains poorly characterized. We reveal that in yeast, overexpressed RNase H1 (*RNH1*) has no effect on gene expression, cell growth, or RNA-DNA hybrid resolution in wild-type cells. Overexpressed RNase H1 does, however, remove RNA-DNA hybrids in mutants where hybrids have become dysregulated. Endogenous RNase H1 becomes up-regulated and chromatin-associated in the absence of Sen1 in a DNA replication checkpoint-dependent manner. Rnh1 gets recruited to genomic loci where RNA-DNA hybrids accumulate following the loss of Sen1. Rnh1, together with Sen1, promotes DNA replication at sites of transcription-replication conflict. Hence, RNase H1, overexpressed or endogenous, responds to unscheduled, stress-inducing RNA-DNA hybrids.

INTRODUCTION

RNA-DNA hybrids form primarily in a co-transcriptional manner when the 5' end of nascent RNA base pairs with the template strand of DNA. Hybrid formation can result in a 3-stranded structure (RNA-DNA hybrid + displaced single-stranded DNA [ssDNA] strand) referred to as an R-loop. RNA-DNA hybrids and R-loops, used interchangeably here for simplicity, have important cellular functions, many of which have only recently been revealed.¹ RNA-DNA hybrids can promote DNA repair through homologous recombination,^{2–5} regulate transcription termination,⁶ contribute to telomere end protection,^{7,8} and influence gene expression through chromatin establishment.^{9,10} Despite their contributions to the above-mentioned nuclear processes, R-loops are surprisingly short lived, with half-lives of approximately 10 min across the human genome.¹¹ This rapid turnover is required to ensure that R-loops do not become a source of genome instability. When RNA-DNA hybrids are not removed in a timely manner in cycling cells, their encounter with the DNA replication machinery can lead to replication stress and DNA strand breaks, both of which can compromise genome integrity.^{12–14} In non-cycling cells, the displaced ssDNA of the R-loop is more prone to damage, mutagenesis, and the formation of secondary structures

when hybrid removal is impaired.^{15,16} Hence, the regulation of RNA-DNA hybrids must be finely tuned, in terms of formation and removal, to ensure that the physiological effects are realized before they develop into sources of chromosomal instability. Although cause and consequence cannot be differentiated, the negative implications of mis-regulated RNA-DNA hybrids are underscored in the myriad of pathological scenarios where R-loop accumulation has been observed.¹³

In general, there are two means to limit/regulate RNA-DNA hybrids: (1) prevent their formation and (2) actively remove them. The formation of hybrids can be prevented through the action of RNA binding proteins that associate with the nascent RNA as it emerges from the exit channel of the respective RNA polymerase and prevent its base pairing with DNA.¹⁷ Examples of such RNA binding proteins include the THO/TREX complex and the spliceosome.^{12,18} In the case that hybrids do form, they can be removed through the action of the RNase H nucleases (RNase H1 and H2)¹⁹ as well as by helicases with RNA-DNA hybrid unwinding capacity. In budding yeast *S. cerevisiae*, the RNase H enzymes, together with the Sen1^{Senataxin} helicase, combine to limit RNA-DNA hybrid levels.²⁰ Sen1 is an essential gene; however, conditional alleles, such as *sen1-1*, can be used to partially inactivate the protein in a temperature-dependent manner.²¹



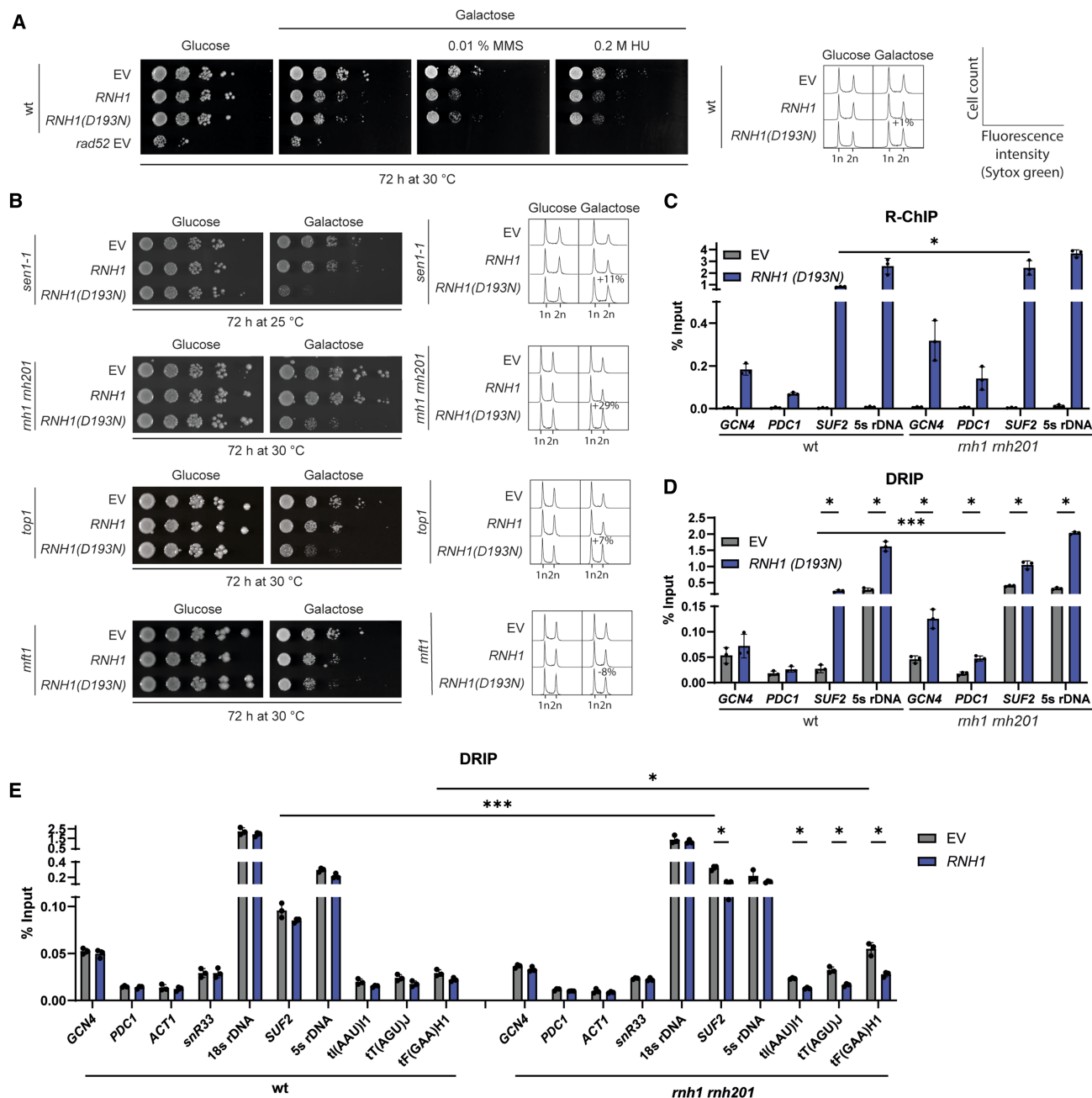


Figure 1. Overexpressed *RNH1* likely acts at misregulated RNA-DNA hybrids

(A) 10-fold serial dilutions of the indicated strains transformed with the indicated plasmids were spotted on SC-Leu plates containing either 2% glucose or galactose. Additionally, galactose-containing plates were supplemented with 0.01% MMS or 0.2 M HU. Images were taken after 3 days at 30°C. Flow cytometry of the same strains was carried out. Strains were grown in SC-Leu + 2% raffinose prior to addition of 2% glucose or galactose. The overexpression was carried out for 5 h at 30°C. A *rad52* control was used as positive control for slow growth and damage sensitivity in spotting assays. EV: empty vector.

(B) 10-fold serial dilutions of the indicated strains transformed with the indicated plasmids were spotted on SC-Leu plates containing either 2% glucose or galactose. Images were taken after 3 days at 30°C for *mh1 mh201*, *top1*, and *mtf1* and at 25°C for *sen1-1*. Flow cytometry of the same strains was carried out. Strains were grown in SC-Leu + 2% raffinose prior to addition of 2% glucose or galactose. The overexpression was carried out for 5 h at 30°C. EV: empty vector. % of G2 cells was calculated as the % ratio of G2:EV in galactose ($n = 2$).

(C) Rnh1 (D193N) ChIP for determining the binding of Rnh1(D193N)-HA to chromatin after overexpression for 8 h in wild-type (WT) and *mh1 mh201* cells. Data are depicted as mean \pm SD, $n = 3$; unpaired t test ($p < 0.05$). EV: empty vector.

(legend continued on next page)

The RNase H enzymes are not essential in unchallenged conditions. However, the absence of both RNase H1 (*RNH1*) and any of the trimeric RNase H2 genes (*RNH201*, *RNH202* and *RNH203*) results in sensitivity to genotoxic agents.²² When all three hybrid resolvases are compromised simultaneously (RNase H1, RNase H2, and Sen1), hybrids strongly accumulate, along with increased levels of DNA damage, checkpoint activation, and cell death.²⁰

When Sen1 function is impaired, R-loops specifically accumulate in the S phase of the cell cycle and delay replication progression, indicating that Sen1 limits R-loops at sites of transcription-replication conflicts (TRCs).²³ Consistently, Sen1 associates and travels with the replisome through its interaction with Ctf4 and Mrc1,²⁴ and this interaction is required to alleviate the TRCs.²⁵ RNase H2 accounts for nearly all RNase H activity in the cell,²⁶ and the majority of RNA-DNA hybrids are removed in an RNase H2-dependent manner.²⁷ Chromosome instability is increased in the absence of RNase H2 but only to negligible levels when RNase H1 is absent.²⁷ We have shown that RNase H2 is able to function outside of S phase to limit the accumulation of RNA-DNA hybrids.²⁸ Recently, it was demonstrated that the Smc5/6 complex can stimulate RNase H2 activity toward R-loops, and genetic evidence from this study also suggests that replication-associated R-loops are not Smc5/6 targets, consistent with either a pre- or post-replicative function for RNase H2 at R-loops.²⁹ In human and yeast cells, it was reported that RNase H2 likely acts in a post-replicative manner to resolve RNA-DNA hybrids behind the replication fork.³⁰

Although we have gained insight into the temporal activity of Sen1 (S phase) and RNase H2 (outside of S phase) toward RNA-DNA hybrids, there is little understanding regarding how RNase H1 is regulated, even though RNase H1 overexpression is regularly employed as a tool to reduce RNA-DNA hybrid levels. Zimmer and Koshland have demonstrated that in yeast, Rnh1 is not responsible for the removal of the bulk of RNA-DNA hybrids and hypothesized that it may only be required at sites where hybrids are particularly stable and lead to chromosome stress.²⁷ Consistently, Rnh1 only suppressed loss of heterozygosity (LOH) events along chromosome III in a region that was particularly prone to hybrid formation. RNase H2, on the other hand, prevented a general LOH increase across the chromosome and was responsible for the majority of R-loop removal.²⁷ Interestingly, that study also reported that Rnh1 has the ability to physically associate with all RNA-DNA hybrids (high or low DNA-RNA immunoprecipitation [DRIP] signal) but is only able to remove them at particularly hybrid-prone regions (high DRIP signal), suggesting that it may be activated locally as part of a stress response.²⁷

We have previously demonstrated that yeast RNase H1 (Rnh1) can function in S and G2 phases of the cell cycle and, in agreement with Zimmer and Koshland²⁷, hypothesized that it may act as a stress-response enzyme. We showed that Rnh1 became more abundant on chromatin when Sen1 was in-

activated.²⁸ Here, we extend our understanding of RNase H1 regulation by demonstrating that (1) when *RNH1* is overexpressed, it gets recruited to many, if not all, genes where hybrids can form, but it only resolves hybrids when they are misregulated; (2) Rnh1 promotes the timely resolution of TRCs in the absence of Sen1 and enhances the viability of *sen1-1* mutants; and (3) endogenous Rnh1 levels increase in a DNA replication checkpoint-dependent manner when Sen1 can no longer resolve TRCs. Our data suggest that Rnh1, whether overexpressed or endogenous, is specifically regulated to resolve R-loops that have become dysregulated and cause stress. In addition, our data suggest that Rnh1 regulation at R-loops may be a two-step process. In the first step, a checkpoint-mediated increase in Rnh1 levels ensures its hybrid association. We hypothesize that the second step, involving Rnh1 activation and subsequent hybrid elimination, only occurs at deregulated hybrids that have resulted in a TRC.

RESULTS

Overexpressed *RNH1* may preferentially act at dysregulated RNA-DNA hybrids

RNase H1 overexpression is frequently employed as a tool to resolve RNA-DNA hybrids *in vivo*. We used a galactose inducible promoter to drive *RNH1* gene expression in budding yeast *S. cerevisiae* (Figure S1A) to gain mechanistic insights regarding the nuances of RNase H1 overexpression. Surprisingly, only minimal effects on cell growth and cell cycle distribution were observed when either active (*RNH1*) or catalytically inactive (*RNH1* D193N) alleles of RNase H1 were overexpressed in unchallenged (galactose) conditions or in the presence of genotoxic stress induced by either MMS (methyl methanesulfonate) or hydroxyurea (HU) (Figure 1A). RNA sequencing of total RNA revealed that, excluding the overexpressed *RNH1* gene itself, zero genes were differentially expressed when *RNH1* was up-regulated, and only two genes were changed following *RNH1* (D193N) overexpression (Figure S1B). Together, we conclude that the overexpression of yeast *RNH1* (active or inactive) has minimal effects on wild-type yeast cells grown in unchallenged conditions.

In contrast to wild-type cells, the overexpression of catalytically inactive *RNH1* (D193N) resulted in a pronounced growth defect in mutants (*sen1-1*, *rnh1 rnh201*, *top1*, *mtf1*) where it has been shown that RNA-DNA hybrids are no longer regulated in a timely manner (Figure 1B).^{18,23,31,32} In the mutants where hybrids are misregulated, we observed an accumulation of cells with a 2n DNA content (% 2n cells indicated) using flow cytometry, consistent with a checkpoint-mediated G2 delay (Figure 1B, compare Galactose EV to Galactose *RNH1* (D193N)). The above results suggest that overexpressed *RNH1* may have more pronounced effects when RNA-DNA hybrids are misregulated and has little effect in wild-type cells when other hybrid prevention and removal pathways are intact.

(D) DRIP for determining the effect of *RNH1*(D193N) overexpression on R-loop levels after 8 h in wild-type (WT) and *rnh1 rnh201* cells. Data are depicted as mean \pm SD, $n = 3$; unpaired t test ($*p < 0.05$, $***p < 0.001$).

(E) DRIP for determining the effect of *RNH1* overexpression on R-loop levels after 3 h in wild type (WT) and *rnh1 rnh201* cells. Data are depicted as mean \pm SD, $n = 3$; unpaired t test ($*p < 0.05$, $***p < 0.001$). EV: empty vector.

To test these notions further, we performed ChIP (chromatin immunoprecipitation) and DRIP using the hemagglutinin (HA) antibody, targeting Rnh1-HA, and the S9.6 antibody to detect overexpressed *RNH1* and RNA-DNA hybrids, respectively. Overexpressed *RNH1* (D193N) associated with all loci tested, and its recruitment to these loci was further increased in the complete absence of RNase H activity (*rnh1 rnh201* cells) (Figures 1C and S1C). DRIP experiments revealed that RNA-DNA hybrids increased at all loci tested when *RNH1* (D193N) was overexpressed in *rnh1 rnh201* mutants, but only at some loci in wild-type cells (Figures 1D and S1D). The accumulation of RNA-DNA hybrids at an increased number of loci in *rnh1 rnh201* mutants may explain why the overexpression of catalytically inactive *RNH1* is specifically toxic in mutants where hybrids are misregulated (Figure 1B). Strikingly, the overexpression of catalytically active *RNH1* did not reduce DRIP signals at any locus tested ($n = 10$) in wild-type cells (Figure 1E) in line with the observation that *RNH1* overexpression has little, or no, effect on cell growth (Figure 1A) or gene expression in wild-type cells (Figure S1B). In contrast, *RNH1* overexpression significantly reduced DRIP signals at many, albeit not all, loci in *rnh1 rnh201* mutant cells. Taken together, these data suggest that overexpression of RNase H1 has little, or no, effect on RNA-DNA hybrids in wild-type cells where other RNA-DNA hybrid resolvases are intact. When hybrids become dysregulated, as in the case of *rnh1 rnh201* mutants, the overexpression of *RNH1* is more likely to promote RNA-DNA hybrid resolution. These results, with overexpressed RNase H1, support the previously proposed hypothesis that RNase H1 is acting in response to misregulated RNA-DNA hybrids and R-loops that result in (replication) stress.^{27,28}

Sen1 loss results in increased Rnh1 levels

While the above data (Figure 1) was related to overexpressed *RNH1*, we wanted to test whether endogenous Rnh1 was also specifically responding to stress inducing/misregulated RNA-DNA hybrids. If Rnh1 is acting at misregulated RNA-DNA hybrids, then its function may become essential in the absence of other R-loop resolvases. In unchallenged conditions, the loss of *RNH1* showed a negative genetic interaction with the temperature-sensitive *sen1-1* mutant at the semi-permissive temperature of 28°C (Figure 2A), while the loss of other RNA-DNA hybrid regulators grew comparably to wild-type cells in the presence or absence of *RNH1* (Figure 2A). Likewise, *sen1-1* mutant cells did not display additional viability defects in the absence of *RNH201* (RNase H2 catalytic subunit) or *TOP1* and showed some growth defects when the THO/TREX complex was mutated (*mft1*) (Figure S2A). In summary, genetic evidence suggests that endogenous Rnh1 may become particularly important for cell viability when Sen1 function is impaired, but not when other R-loop resolvases are absent.

To further interrogate the relationship between Sen1 and Rnh1, we assayed protein levels when one, or the other, factor was inactivated. Using an auxin-inducible degron to deplete Sen1 (Sen1-AID*), we observed that endogenous Rnh1 protein levels increased approximately 5-fold in a time-dependent manner following the addition of the auxin analog IAA (3-indoleacetic acid) (Figures 2B and 2C, gray bars). The increase in

endogenous Rnh1 levels was strongly reduced when an additional copy of *RNH1* (Rnh1-MYC) was overexpressed from an ectopic plasmid to remove hybrids (Figure 2C, blue bars), suggesting that the accumulation of RNA-DNA hybrids was triggering Rnh1 accumulation. Interestingly, Sen1 protein levels also increased, albeit to a lesser extent, when *RNH1*, but not *RNH201*, was deleted, revealing a potential regulatory crosstalk between the proteins (Figure S2B). We previously demonstrated that Rnh1 localizes to chromatin in *sen1-1* mutant cells at non-permissive temperatures.²⁸ Chromatin localization of Rnh1 was re-capitulated in the Sen1-AID* background, where we observed that increased Rnh1 protein levels were occurring specifically on the chromatin, and not the soluble, fraction (Figure 2D).

Importantly, the up-regulation of Rnh1 was specific to the loss of Sen1 function as Rnh1 levels did not increase following the loss of Rnh201, Hpr1 (THO complex), or Top1 when the respective degron fusions were depleted (Figure S1C). Furthermore, Rnh201 and Rnh202 levels did not increase when Sen1-AID* was inactivated (Figure S2D). Interestingly, neither the addition of HU nor MMS caused an increase in Rnh1 levels (Figure S2E). Finally, the depletion of another essential gene, Cdc20, did not trigger the up-regulation of Rnh1, ruling out that the effect seen in the absence of Sen1 is due to its essential nature (Figure S2F). Hence, there are very specific reciprocal genetic (Figures 2A and S2A) and regulatory (Figures 2B–2D) interactions between Sen1 and Rnh1. Furthermore, like overexpressed *RNH1*, which likely targets misregulated R-loops, endogenous Rnh1 may specifically respond to Sen1-targeted R-loops.

To assess the interplay of Sen1 and Rnh1 on global RNA-DNA hybrid levels, we performed a dot-blot assay on total nucleic acids with the S9.6 antibody (Figures 2E and 2F). Interestingly, there was only a slight increase in signal in the absence of Sen1, but this was increased further when *RNH1* was additionally deleted (Figures 2E and 2F). Hence, the up-regulation of *RNH1* (Figure 2C) may compensate to keep R-loops in check in Sen1's absence.

To determine if Rnh1 is specifically targeting Sen1-regulated R-loops, we analyzed published DNA-RNA immunoprecipitation followed by cDNA conversion coupled to high-throughput sequencing (DRIPc-seq) data comparing hybrid levels between wild-type and Sen1-AID-depleted cells²³ in S phase. We identified the top 12 loci that accumulated hybrids following Sen1 loss (see Figures S3A and S3B for examples) and determined if endogenously expressed catalytically dead Rnh1 gets recruited to those loci using ChIP. Indeed, upon Sen1 depletion through IAA, Rnh1 was recruited to all protein-coding regions demonstrated to be Sen1 targets (Figures 2G and S3C). In the absence of Sen1, overexpressed *RNH1* can remove hybrids at these loci when overexpressed,²³ consistent with our prediction that overexpressed *RNH1* targets misregulated R-loops (Figure 1). Although R-loops accumulate to similar extents and at the same loci, but rather in G1, upon Hpr1 depletion,²³ we could not detect Rnh1 at these loci (Figure S3D). The depletion of Rnh201 also did not result in an increased ChIP signal above background (no antibody) levels (Figure S3D). All together, these results indicate that there is a specific interplay between Sen1 and Rnh1 both in terms of genetic interactions as well as regulation of protein abundance and localization. Rnh1 may be working

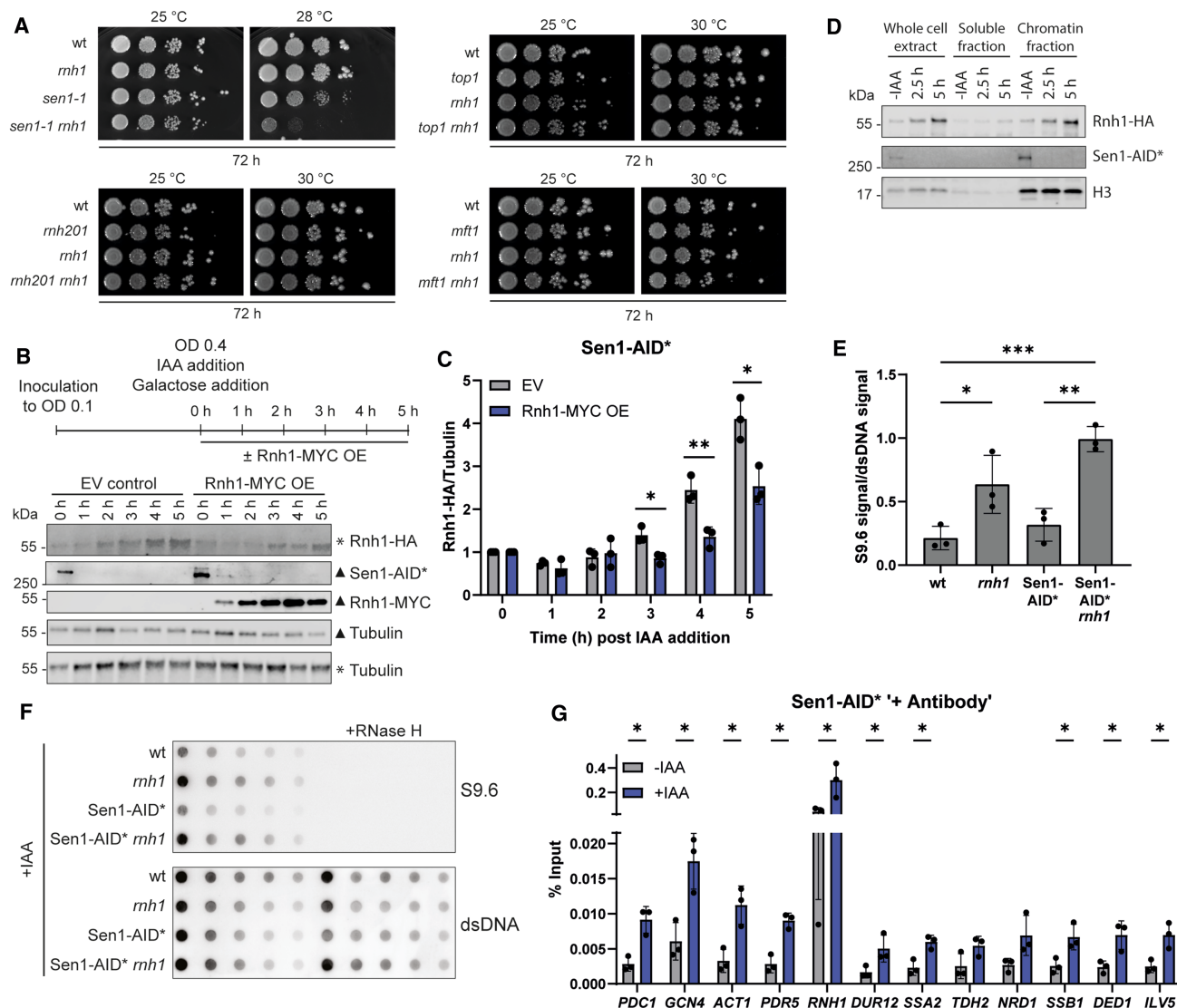


Figure 2. Sen1 loss results in increased Rnh1 levels

(A) 10-fold serial dilutions of the indicated strains were spotted on YPD plates and incubated at indicated temperatures for 3 days.

(B) Western blot analysis of endogenous Rnh1-HA levels over a time course of 5 h after depleting Sen1 and inducing overexpression of Rnh1-MYC. Loading controls for the blots are indicated by the corresponding symbol (▲ or *). EV: empty vector.

(C) Quantification of (B). Values were normalized to the 0 h time point. Data are depicted as mean ± SD, $n = 3$; unpaired t test (* $p < 0.05$; ** $p < 0.01$). EV: empty vector.

(D) Western blot analysis of cell fractionation into whole-cell extract, soluble protein, and chromatin-associated protein. Exponentially growing yeast were either untreated or grown for 2.5 h or 5 h in 1 mM IAA for depletion of Sen1-AID*.

(E) Quantification of (F). The S9.6 signal was normalized to the dsDNA signal. Data are depicted as mean ± SD, $n = 3$; unpaired t test (* $p < 0.05$; ** $p < 0.01$, *** $p < 0.001$).

(F) Dot blot for RNA:DNA hybrid levels upon Sen1-AID* depletion for 5 h in 1 mM IAA.

(G) Chromatin immunoprecipitation of endogenous catalytically inactive Rnh1-HA in a Sen1-AID* background after 5 h of IAA treatment or without treatment. Data are depicted as mean ± SD, $n = 3$; unpaired t test (* $p < 0.05$).

together with Sen1 or compensating for the loss of function of Sen1, at transcription-replication conflicts.

Rnh1 levels increase in an RNAPII-dependent manner

The Nrd1-Nab3-Sen1 (NNS) complex promotes transcription termination at over 1,000 non-coding RNAs.^{33–35} Loss of NNS

function leads to both direct and indirect global transcription deregulation due to aberrant readthrough at these loci.³⁶ To determine if Sen1 may be directly affecting the transcription termination of the *RNH1* gene itself, we performed 3' RACE (rapid amplification of cDNA ends) on total RNA from strains where the NNS complex had been depleted (Figures 3A, 3B,

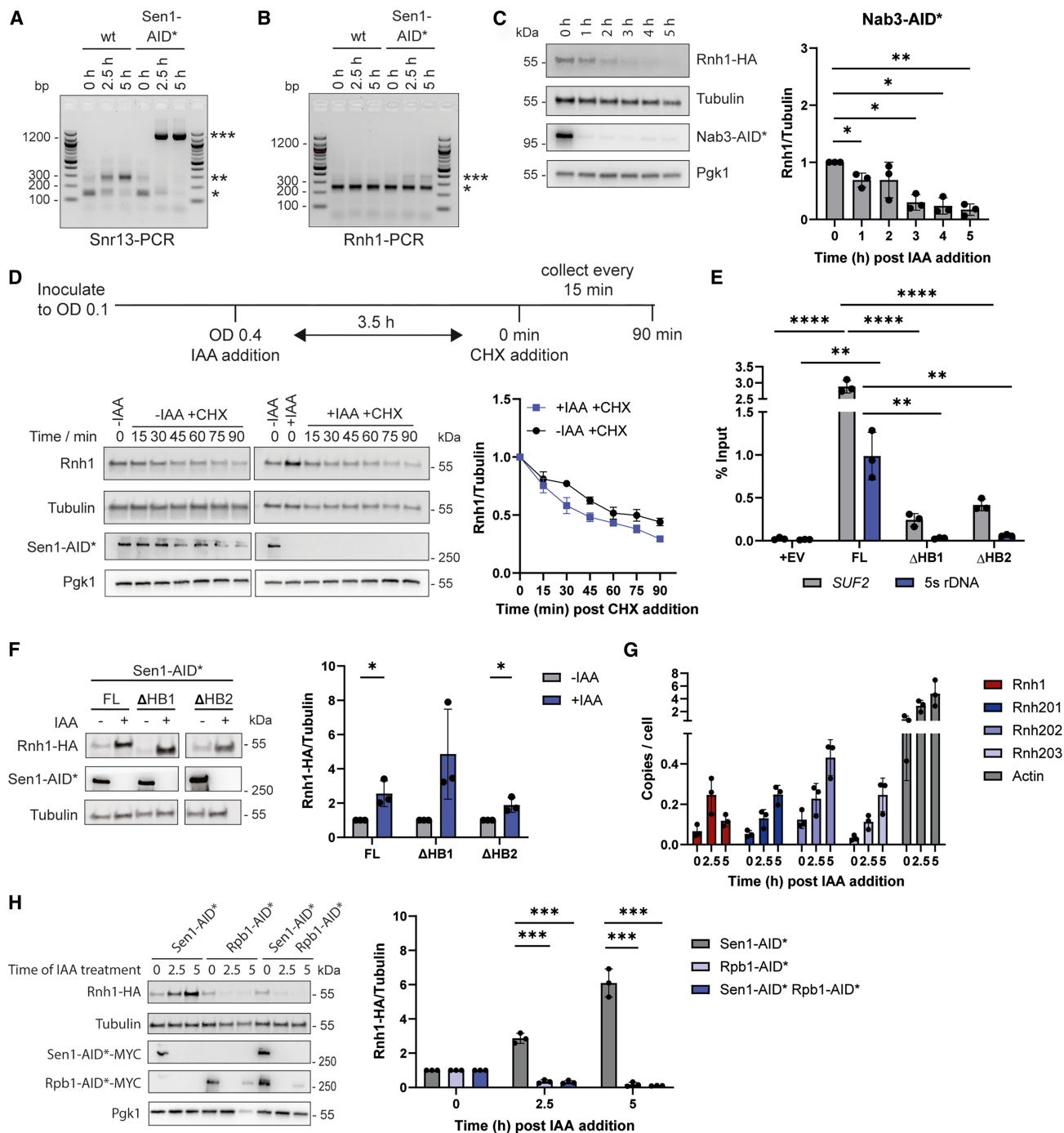


Figure 3. Sen1 loss triggers an RNAPII-dependent induction of *RNH1*

(A) 3' RACE analysis of transcription termination. The cells were grown to exponential phase and treated with 1 mM IAA. Samples were collected before IAA addition, after 2.5 h and 5 h of treatment. The PCR analysis was carried out at the *SNR13* gene, a known readthrough locus in Sen1-deficient cells used here as positive control (*expected PCR product size; **effect of IAA; ***readthrough product).

(B) 3' RACE analysis of transcription termination. The cells were grown to exponential phase and treated with 1 mM IAA. Samples were collected before IAA addition, after 2.5 h and 5 h of treatment. The PCR analysis was carried out at the *RNH1* gene (*expected PCR product size; ***readthrough product).

(C) Western blot analysis of endogenous Rnh1-HA levels over a time course of 5 h after depleting Nab3-AID*. Values were normalized to the 0 h time point. Data are depicted as mean \pm SD, $n = 3$. Paired t test (* $p < 0.05$; ** $p < 0.01$).

(legend continued on next page)

S4A, and S4B). As expected, following depletion of Sen1, Nab3, or Nrd1, the *SNR13* small nucleolar RNA (snoRNA) showed a termination defect, as seen by the increased 3' RACE product (Figures 3A and S4A). In contrast, the 3' termination site of the *RNH1* gene was not affected upon NNS loss (Figures 3B and S4B). In agreement with the loss of Sen1's NNS function not being responsible for Rnh1 up-regulation, neither the loss of Nrd1 nor Nab3 led to increased Rnh1 protein levels (Figures 3C and S4C).

To test whether Rnh1 up-regulation was due to changes in protein stability, we used cycloheximide (CHX) to inhibit translation, combined with Sen1-AID* inactivation to determine if the rate of Rnh1 turnover may be affected. Sen1 was inactivated for 3.5 h to allow Rnh1 levels to accumulate before adding CHX and taking samples for whole-cell protein extraction (Figure 3D). Levels of Rnh1 were increased at time "0" in the presence of IAA, as expected; however, the rate of degradation relative to tubulin was unchanged, regardless of the presence or absence of Sen1 (Figure 3D). Since Rnh1 strongly accumulates on chromatin upon Sen1 loss (Figure 2D), we entertained the notion that exclusively the chromatin-bound fraction of Rnh1 may be stabilized. To address this, we created Rnh1 alleles that were missing one or the other RNA-DNA hybrid binding domains (HB1 or HB2) to impair chromatin association (Figure S4D). Upon overexpression of these alleles, we could verify that they were strongly affected in their ability to associate with RNA-DNA hybrids, as revealed through ChIP experiments (Figure 3E). We constructed endogenously expressed versions of the hybrid binding impaired alleles in a Sen1-AID* background. Both the HB1- and HB2-deleted *RNH1* alleles were up-regulated upon IAA addition, indicating that the increase in Rnh1 levels was not linked to hybrid binding per se (Figure 3F).

We tested whether the transcriptional regulation of *RNH1* may be accountable for increased levels following loss of Sen1. Reverse transcription droplet digital PCR (RT-ddPCR) revealed that loss of Sen1 function led to increased *RNH1* mRNA levels (Figure 3G). However, as previously mentioned, Sen1 has pleiotropic effects on transcription throughout the genome. Indeed, all three RNase H2 subunits, as well as actin (*ACT1*) mRNAs were also up-regulated following IAA addition (Figure 3G), while their protein levels remained unchanged (Figure S2D). Therefore, it is difficult to discern whether the increased transcription of the *RNH1* gene is specific. Nonetheless, when transcription was inhibited through the depletion of the Rpb1 subunit of RNAPII, at the same time that Sen1 was depleted, we were unable to detect

an increase in Rnh1 levels (Figure 3H). Together, these data suggest that *RNH1* is transcriptionally induced following the loss of Sen1, which accounts for increased protein levels and subsequent chromatin association.

The replication checkpoint is required for Rnh1 accumulation

As Rnh1 levels were not responding to the loss of NNS function (Figure 3), we tested whether the loss of Sen1's replication function^{23–25} might trigger Rnh1 accumulation. In support of this, by preventing S phase entry through G1 arrest, the increase in Rnh1 levels was prevented following Sen1 degradation (Figures 4A and 4B). Furthermore, in mutants expressing the *sen1-3* allele,²⁴ where association to the replisome is impaired, there was a negative genetic interaction between *sen1-3* and the deletion of *RNH1*, but not between the deletion of *RNH201* and *sen1-3*, in the presence of MMS (Figure 4C). In addition, Rnh1 levels increased in the presence of the *sen1-3* allele (Figure 4D), albeit not to the same extent as we observed when Sen1 was completely degraded (Figure 2). In summary, Rnh1 does not respond to loss of Sen1 if cells are prevented from entering S phase, and the specific loss of Sen1 function at replisomes results in Rnh1 accumulation and a negative genetic interaction in *rnh1*-deletion cells. Together, these results suggest that Rnh1 and Sen1 collaborate at RNA-DNA hybrids during DNA replication.

Replication stress can locally activate the intra-S phase checkpoint, which in yeast is transduced via Mec1^{ATR} and the downstream effector kinase Rad53^{Chk1}. The mediator proteins Rad9 and Mrc1 act in a partially redundant manner to amplify the phosphorylation and activation of Rad53. While the depletion of Mec1 with an AID* tag was technically problematic, when Rad53 was inactivated in addition to Sen1 loss, the accumulation of Rnh1 was completely suppressed (Figure 4E). Even in the presence of Sen1, Rad53 appears to contribute to the maintenance of Rnh1 levels (Figure 4E). Loss of both Mrc1 and Rad9 together, but not individually, also prevented Rnh1 accumulation (Figure 4F). The loss of Tel1^{ATM} and Chk1, on the other hand, had no influence on Rnh1 accumulation following Sen1 degradation (Figures S5A and S5B). Consistent with the up-regulation of *RNH1* being dependent on transcription induction, *RNH1* mRNA levels were slightly reduced upon Rad53 depletion even in *SEN1** cells (Figure S5C).

As the increase of Rnh1 levels is linked to chromatin association, we tested whether Rad53 was also required for the

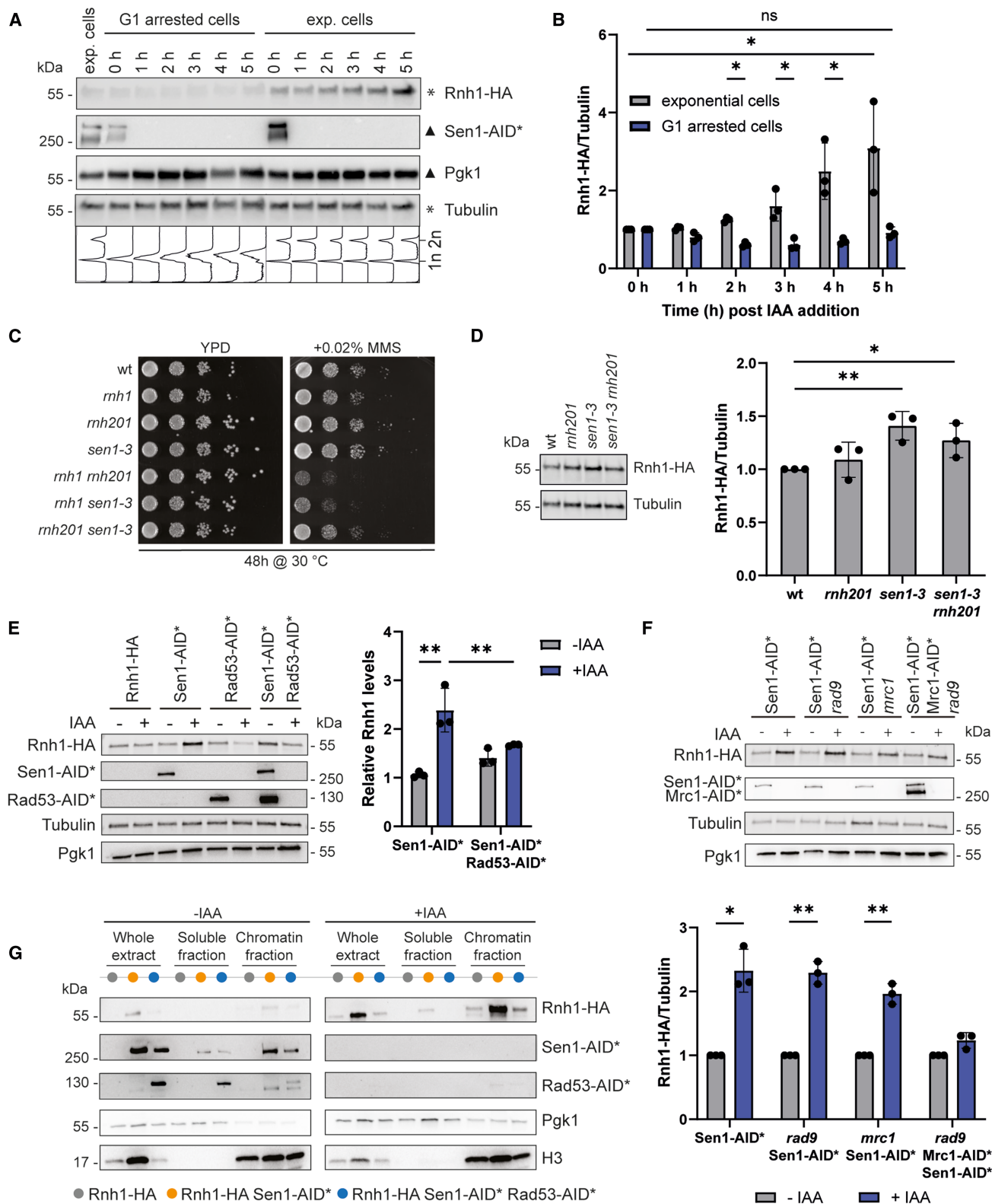
(D) Protein stability of RNase H1 determined by cycloheximide chase assay. The cells were grown to exponential phase and 1 mM IAA was added. After 3.5 h, 200 µg/mL cycloheximide (CHX) was added, and samples were collected every 15 min for 90 min. The protein levels of Rnh1 were determined by western blot analysis. Data are depicted as mean ± SD, *n* = 3.

(E) Rnh1 (D193N) ChIP for determining the binding of overexpressed Rnh1(D193N)-HA upon loss of hybrid binding domain 1 or 2 in *rnh1 rnh201* cells. Cells were grown in SC-Ura until they reached exponential phase. Overexpression was induced for 2 h by addition of 2% galactose. EV: empty vector; FL: full-length Rnh1(D193N); ΔHB: deletion of hybrid binding domain. Data are depicted as mean ± SD, *n* = 3; unpaired *t* test (***p* < 0.01; *****p* < 0.0001).

(F) Western blot analysis of endogenous Rnh1-HA levels in a Sen1-AID* strain depending on deletions of hybrid binding domains 1 and 2 of Rnh1. Cells were treated for 5 h with or without 1 mM IAA. FL: full-length Rnh1; ΔHB, deletion of hybrid binding domain. Values were normalized to the –IAA samples. Data are depicted as mean ± SD, *n* = 3; unpaired *t* test (**p* < 0.05).

(G) Transcript copy number determination by digital droplet PCR (ddPCR). The cells were grown to exponential phase and treated with IAA to deplete Sen1. Samples were collected before IAA addition, after 2.5 h and 5 h of treatment. Data are depicted as mean ± SD, *n* = 3.

(H) Western blot analysis of endogenous Rnh1-HA levels over a time course of 5 h after depleting Sen1-AID* and/or Rpb1-AID*. Values were normalized to the 0 h time point. Data are depicted as mean ± SD, *n* = 3; unpaired *t* test (***p* < 0.001).



(legend on next page)

accumulation of Rnh1 on chromatin. Indeed, Rnh1 was no longer recruited to chromatin when Rad53 was depleted in addition to Sen1 (Figure 4G, compare final 2 lanes). Importantly, although Sen1 and Rad53 are both essential genes, their co-depletion for the course of these experiments (5 h) did not have a detectable influence on cell viability (Figure S5D). Together, we have demonstrated that Rnh1 is being regulated in response to the loss of Sen1's functions in S phase in a manner dependent on the Rad53-mediated replication checkpoint.

Rnh1 promotes replication through TRCs in the absence of Sen1

Based on the above results, we predicted that Rnh1 would contribute to a timely replication completion in the absence of Sen1 by promoting replication at TRCs through its up-regulation. To get a global picture of replication timing, we used flow cytometry in synchronized cells to verify that the progression through S phase was impaired following IAA addition in the Sen1-AID* strain grown at 25°C (Figure 5A). When *RNH1* was deleted in addition, there was a further delay in replication progression (best seen between 40 and 60 min post G1 release). To determine if Rnh1 specifically acts at TRCs to promote replication, we employed a previously established imaging-based approach for monitoring replication fork progression during transcription-replication encounters in individual live yeast cells.³⁷ Specifically, we monitor replication by tracking the intensity changes of *lacOx128* and *tetOx160* fluorescently labeled arrays integrated in the vicinity of an early-replicating origin, *ARS413*, by time-lapse microscopy (Figure 5B). To measure TRC-associated replication slowdown, we integrated an inducible mouse antisense of IGF2R non-coding RNA (mAIRN) gene in the path of the replisome in a co-directional orientation. Measuring the time interval between the *lacO* and *tetO* array duplication events (e.g., replication-time [Figures 5C and 5D]) in the absence or presence of mAIRN transcription allows us to detect slowdown of single replisomes during an inducible TRC.^{37,38} Using this system, we found that mAIRN induction did not affect replication fork progression in either the presence or absence of the *RNH1* gene in Sen1-AID cells in the absence of IAA (Figure 5C). However, when Sen1-AID was depleted in the presence of IAA, there was a small, albeit non-significant, increase in the replication time of the TRC, indicating a mild replication slow-

down (Figures 5D and S6A). Interestingly, the additional deletion of *RNH1* in the presence of Sen1-AID depletion further slowed down replication and resulted in a statistically significant difference in replication times when compared to the uninduced (non-transcribed) conditions (Figure 5D). Therefore, Rnh1 becomes important for replisome progression when TRCs accumulate upon Sen1 depletion. Additionally, we exploited the fact that a deletion of the *SPT2* genes, which promotes RNAPII elongation, reduces TRCs in the absence of Sen1.³⁹ We combined the *spt2* mutant with *sen1-1* and the combination of *sen1-1* and *RNH1* deletion. In both cases, the reduction of TRCs had a positive effect on the viability (Figure 5E). Furthermore, in the absence of *SPT2*, RNase H1 upregulation is reduced upon Sen1-AID* depletion (Figure S6B). These further support the notion that RNase H1 assists Sen1 at resolving TRCs to promote timely replication completion.

DISCUSSION

Exogenous sources of DNA damage, including UV light, ionizing radiation, as well as various chemicals can break, fragment, and modify chromosomes, leading to compromised genomic integrity and susceptibility to pathologies and premature aging. Exogenous DNA damage can be controlled, to an extent, through lifestyle changes and the avoidance of the respective damaging source. DNA is also at risk of being damaged through normal cellular processes, referred to as endogenous sources of damage. Endogenous DNA damage can arise through processes such as oxidation, alkylation, DNA replication, and transcription, to mention a few. Transcription and DNA replication both occupy the same DNA substrate, and these multi-subunit complexes need to be coordinated to avoid unscheduled collisions. RNA-DNA hybrids and R-loops form downstream of transcription and can lead to transcriptional stalling, thereby increasing the probability that a collision will occur. TRCs result in DNA breakage, replication stress, and aberrant DNA repair.¹² In this study, we show that the RNase H1 enzyme specifically responds to TRCs that accumulate in the absence of Sen1. When Sen1 function is lost, Rnh1 levels accumulate, driving its recruitment to chromatin in a manner that depends on the Rad53 replication checkpoint kinase. Rnh1 functions to ensure a timely completion of DNA replication in the face of unresolved TRCs. Our data

Figure 4. The replication checkpoint is required for Rnh1 accumulation

- (A) Western blot analysis comparing Rnh1 levels in exponential vs. G1 arrested cells after Sen1-AID* depletion. Exponentially growing cells were split and either kept in exponential phase by diluting or arrested in G1 phase by adding 0.24 μ M alpha-factor (experiment carried out in *bar1 Δ* cells). After 1.5 h of arrest, 1 mM IAA was added. Samples were collected for 5 h every hour. Loading controls for the blots are indicated by the corresponding symbol (Δ or \circ).
- (B) Quantification of (A). Values were normalized to 0 h time point. Data are depicted as mean \pm SD, $n = 3$; multiple t tests ($^*p < 0.05$).
- (C) 10-fold serial dilutions of the indicated strains were spotted on YPD plates containing with or without 0.02% MMS. Images were taken after 2 days at 30°C.
- (D) Western blot analysis comparing Rnh1 levels in the context of the *sen1-3* and *mnh201* mutants. Values were normalized to WT. Data are depicted as mean \pm SD, $n = 3$; unpaired t test ($^*p < 0.05$; $^{**}p < 0.01$).
- (E) Western blot analysis of Rad53 dependency of Rnh1 upregulation in Sen1-AID*. Samples were grown to exponential phase, the -IAA samples were taken, and 1 mM IAA was added. The cells were incubated for 5 h, and the +IAA samples were taken. For quantification, the Sen1-AID* samples were normalized to the Rnh1-HA samples, and the Sen1-AID* Rad53-AID* samples were normalized to the Rad53-AID* samples. Data are depicted as mean \pm SD, $n = 3$; two-way ANOVA ($^{**}p < 0.01$).
- (F) Western blot analysis of S-phase checkpoint adaptor dependency of Rnh1 upregulation in Sen1-AID*. Samples were grown to exponential phase, the -IAA sample was taken, and 1 mM IAA was added. The cells were incubated for 5 h, and the +IAA sample was taken. Values were normalized to -IAA samples. Data are depicted as mean \pm SD, $n = 3$; multiple paired t tests ($^*p < 0.05$, $^{**}p < 0.01$).
- (G) Fractionation assay for detecting Rnh1 levels in the chromatin bound fraction vs. soluble fraction. Cells were grown as described in (E).

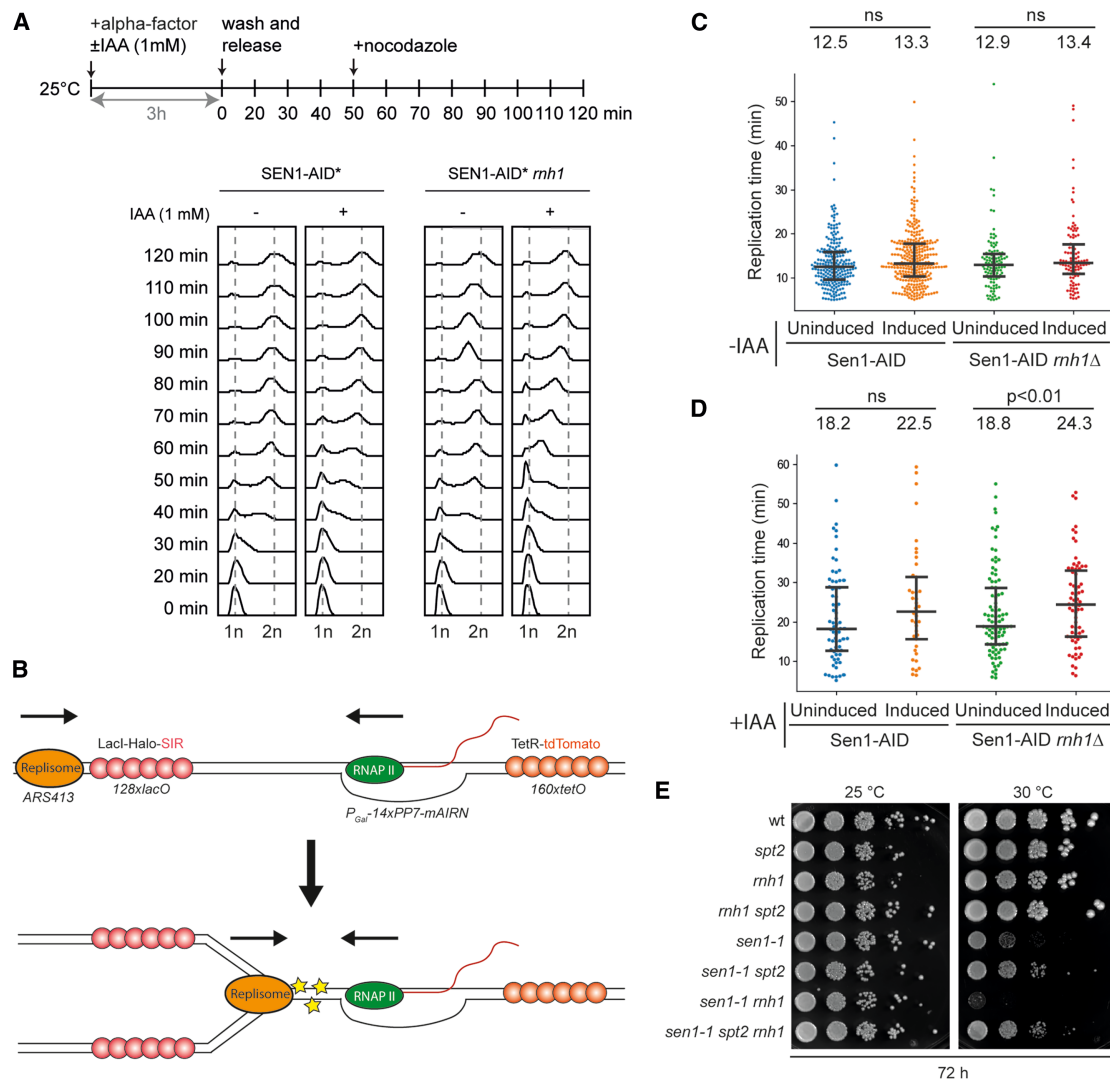


Figure 5. Rnh1 assists with timely replication completion through TRCs

(A) S-phase progression studied by DNA content in flow cytometry. Exponential cultures grown in YPD at 25°C were arrested in G1 with 2 μ g/mL alpha-factor in the first hour and 4 μ g/mL alpha-factor in subsequent hours for 3 h with or without addition of 1 mM IAA in the beginning of synchronization. Cells were washed twice in H₂O with or without IAA and were released into YPD with or without IAA. 50 min after release, 15 μ g/mL nocodazole was added from a 1.5 mg/mL stock in DMSO for arresting the cells in G2. The DNA content was analyzed by flow cytometry.

(B) Schematic representation of the system for measuring replication during inducible TRCs. Replication fork progression is monitored using two operator arrays, 128x*lacO* and 160x*tetO*, integrated downstream of *ARS413*, labeled by LacI-Halo-SiR and TetR-TdTomato. For monitoring replisome progression during TRC, mAIRN under the pGal promoter is integrated in a co-directional or head-on orientation between the arrays (for illustration purposes only, the head-on orientation is presented). Collisions between the moving replisome and the actively transcribing mAIRN gene could result in harmful TRCs leading to replication slow-down.

(C) Replisome progression is not affected by mAIRN transcription in the presence or absence of Rnh1. Replication times in individual WT or *mh1* cells measured in the absence of IAA and in either the absence or the presence of mAIRN transcription. The mAIRN gene is located in a co-directional orientation relative to replisome progression.

(D) Replisome progression is slowed down in Sen1-AID-depleted and *mh1* mutant cells upon mAIRN induction. Replication times in individual Sen1-AID-depleted or Sen1-AID-depleted and *mh1* mutant cells, measured in the presence of IAA and in either the absence or the presence of co-directional mAIRN transcription.

(E) 10-fold serial dilutions of the indicated strains were spotted on YPD plates and incubated at indicated temperatures for 3 days.

suggest that in unchallenged conditions, Rnh1 makes minor contributions at TRCs (Figure 5) through RNA-DNA hybrid resolution (Figure 2F), with Sen1 playing a more prominent role in displacing the transcription machinery (Figure 6A). When Sen1 is absent, Rnh1's function to resolve RNA-DNA hybrids at TRCs

becomes more important (Figure 5D), and accordingly, it is upregulated and eventually activated at TRCs to promote hybrid resolution and timely replication completion (Figure 6B).

There are two evolutionarily conserved RNase H enzymes (H1 and H2). However, the division of labor between the enzymes is

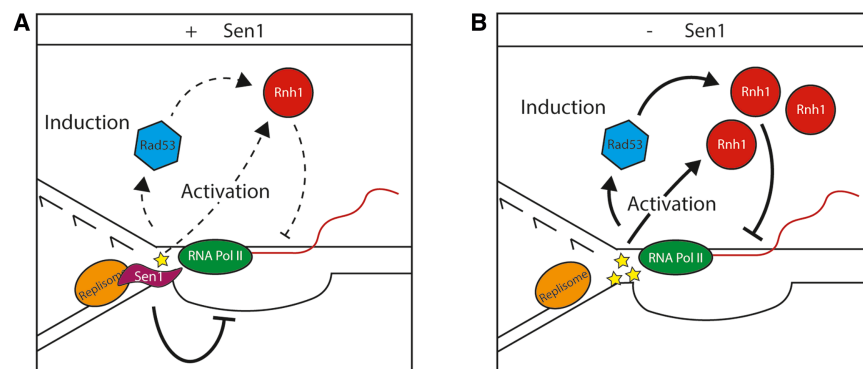


Figure 6. Interplay of Sen1 and Rnh1 during TRCs

(A) Sen1 is the main contributor to deal with TRCs, with minor (dashed lines) contributions from Rnh1 to remove TRC-associated RNA-DNA hybrids.

(B) In the absence of Sen1, unresolved TRCs lead to stronger checkpoint activation and *RNH1* up-regulation. Rnh1-mediated removal of the RNA-DNA hybrid becomes more important in the absence of Sen1 function, to ensure the timely completion of DNA replication through the TRC.

poorly understood. Previous studies from the Koshland lab have determined that the majority of RNA-DNA hybrids are removed in an RNase H2-dependent manner, whereas Rnh1 contributes very little to hybrid removal in unperturbed conditions.²⁷ Accordingly, using chromosome III LOH as a readout, the LOH events were strongly elevated and evenly distributed along the entire chromosome in the absence of RNase H2. When *RNH1* was deleted, LOH events were only slightly increased and concentrated in a region of chromosome III that is particularly prone to RNA-DNA hybrid formation.²⁷ ChIP experiments revealed that Rnh1 associates with all hybrids along the chromosome, but when *RNH1* was removed, LOH was only unleashed at the hybrid-prone region.²⁷ They predicted that Rnh1 may only get activated in a local manner at unscheduled or particularly stable R-loops that induce some sort of stress. In agreement, a parallel study determined that when transcription was altered by mutating RNA biogenesis factors, there was a synergistic increase in LOH following the loss of *RNH1*.⁴¹

We could verify the prediction that Rnh1 only acts at unscheduled R-loops by using an overexpression system. Interestingly, the overexpressed version of catalytically dead Rnh1 could be cross-linked to all loci that we tested (Figure 1). This experiment demonstrated that an important aspect of Rnh1 regulation may be related to its expression levels, as *RNH1* up-regulation is sufficient to promote chromatin association. Our observations with ectopic RNase H1 overexpression appear to be physiologically relevant, as endogenous *RNH1* protein levels also increased when Sen1 function, and hence TRC management, was impaired (Figure 2). Therefore, the amount of cellular Rnh1 seems to be an important step regarding Rnh1 function to ensure it goes to chromatin. Although ectopically overexpressed *RNH1* was recruited to multiple transcribed loci, subsequent DRIP experiments showed that, in wild-type cells, RNA-DNA hybrid levels were not decreased (Figure 1), consistent with the Zimmer and Koshland study.²⁷ We observed that hybrid levels were only significantly decreased at a subset of loci in *rnh1 rnh201* cells when *RNH1* was overexpressed (Figure 1). Therefore, we suggest that Rnh1 may only resolve hybrids that are dysregulated, as previously hypothesized.²⁷ Further support for this model comes from the Aguilera lab, who observed that the decrease in hybrid levels upon Rnh1 overexpression is mild in wild-type

cells but is quite dramatic in the absence of Sen1 or Hpr1 (THO complex).²³ These results also have important implications for the use of RNase H1 overexpression as a tool to reduced hybrid levels. Our data suggest that Rnh1 overexpression will be most effective in mutants where RNA-DNA hybrids are dysregulated and cause replication stress, but using it to probe the function of endogenous R-loops may not be effective as these hybrids are likely removed by other resolvases such as RNase H2 and Sen1.

We postulated that DNA replication stress may be the trigger required to increase Rnh1 levels. Consistent with this notion, we could prevent Rnh1 levels from increasing by abolishing the checkpoint response through Rad53 inactivation. Checkpoint inhibition also resulted in lower Rnh1 levels in otherwise wild-type cells, both at the level of the transcript and the protein, suggesting that scheduled TRCs may regularly occur that require Rnh1 activity. Importantly, checkpoint activation per se is not sufficient to stimulate *RNH1* transcription, as the addition of MMS or HU to the media did not result in higher Rnh1 protein levels, despite clear checkpoint activation. Therefore, there may be a particular feature of TRCs that directs the checkpoint to activate *RNH1* transcription. We predict that components of the transcription machinery or the presence of the nascent transcript itself may alter the checkpoint response in such a manner. These ideas remain to be investigated and will be pursued in future studies.

In summary, we have shown that overexpressing Rnh1 is sufficient to promote its association with RNA-DNA hybrids, but not sufficient to trigger the removal of hybrids. We suggest that increased levels of Rnh1, combined with a replication stress-inducing R-loop, are required to trigger hybrid resolution (Figure 1). We propose that in a physiological setting, TRCs weakly activate the DNA damage checkpoint, which is required to drive *RNH1* expression in wild-type, and to a much greater extent, in Sen1-depleted cells (Figure 6). Based on our overexpression results (Figure 1), the association of Rnh1 with chromatin is not sufficient to trigger RNase H activity, we hypothesize that a stress presumably stemming from TRC is also required for local Rnh1 activation (Figure 6, arrows emanating from the replication stress). These results will contribute further to understanding how transcription as a source of endogenous genome instability is dealt with and may be relevant for certain disorders where TRCs are prevalent.

Limitations of the study

We made the general prediction that overexpressed Rnh1 acts more efficiently in mutants where RNA-DNA hybrids are stabilized and hence stress inducing. This, however, was based on 10 loci, and we appreciate that a thorough genome-wide DRIP-seq using various mutants involved in R-loop stabilization would be required to make a definitive conclusion. In Figure 3, we showed that the depletion of Rpb1 prevented the increase in Rnh1 levels, which supported RNAPII transcription being required. It is, however, possible that this prevents TRCs and this is what prevents increased Rnh1 levels. Deciphering between the two possibilities is not possible with the current data.

RESOURCE AVAILABILITY

Lead contact

Requests for further information and resources should be directed to and will be fulfilled by the lead contact, Brian Luke (brialuke@uni-mainz.de).

Materials availability

All unique/stable reagents generated in this study are available from the lead contact with a completed materials transfer agreement.

Data and code availability

- RNA-seq data have been deposited at NCBI's Sequence Read Archive (SRA) as SRA: PRJNA1212884 (see [key resources table](#)) and are publicly available as of the date of publication. All other data are available in the main text or [supplemental information](#).
- This paper does not report original code.
- Any additional information required to reanalyze the data reported in this paper is available from the lead contact upon request.

ACKNOWLEDGMENTS

We thank the Luke lab members for support and discussions and the media lab, flow cytometry, genomics, and protein production core facilities of the IMB. The labs of B.L., H.D.U., and F. Butter are funded by the Deutsche Forschungsgemeinschaft (DFG, German Research Foundation), project ID 393547839 – SFB 1361; and B.L.'s lab is additionally funded by project ID 491145305 – GRK 2859/1 and project ID 552129721. Work in the Hamperl laboratory is supported by the Helmholtz Association, the German Research Foundation (DFG; project ID 552129721), and the European Research Council (ERC starting grant 852798). The lab of A.A. is funded by DFG grant numbers 552129721 and 548574498.

AUTHOR CONTRIBUTIONS

Conceptualization, B.L., C.B.W., and F. Bento; methodology, C.B.W., F. Bento, and M.L.; investigation, C.B.W., M.L., F. Bento, S.G.S., N.S., R.P.W., and M.W.; writing – original draft, B.L. and C.B.W.; writing – review & editing, B.L., H.D.U., A.A., and S.H.; funding acquisition, B.L., H.D.U., and F. Butter; and supervision, B.L., F. Butter, S.H., A.A., and H.D.U.

DECLARATION OF INTERESTS

The authors declare no competing interests.

STAR★METHODS

Detailed methods are provided in the online version of this paper and include the following:

- [KEY RESOURCES TABLE](#)
- [EXPERIMENTAL MODEL AND STUDY PARTICIPANT DETAILS](#)
- [METHOD DETAILS](#)

- Yeast strain generation
- Cell-cycle arrest and release
- Western blot
- DNA content flow cytometry
- RNA extraction
- Reverse transcription
- Digital droplet PCR
- RNA-seq
- RT-qPCR
- 3'RACE
- Chromatin immunoprecipitation
- Spotting assay
- CHX chase assay
- Chromatin binding assay
- Dotblot for measuring RNA:DNA hybrid levels
- Microscopy

• QUANTIFICATION OF MICROSCOPY EXPERIMENTS AND STATISTICAL ANALYSIS

SUPPLEMENTAL INFORMATION

Supplemental information can be found online at <https://doi.org/10.1016/j.celrep.2025.116565>.

Received: January 20, 2025

Revised: August 5, 2025

Accepted: October 27, 2025

REFERENCES

1. Niehrs, C., and Luke, B. (2020). Regulatory R-loops as facilitators of gene expression and genome stability. *Nat. Rev. Mol. Cell Biol.* 21, 167–178. <https://doi.org/10.1038/s41580-019-0206-3>.
2. Ohle, C., Tesorero, R., Schermann, G., Dobrev, N., Sinning, I., and Fischer, T. (2016). Transient RNA-DNA Hybrids Are Required for Efficient Double-Strand Break Repair. *Cell* 167, 1001–1013.e7. <https://doi.org/10.1016/j.cell.2016.10.001>.
3. D'Alessandro, G., Whelan, D.R., Howard, S.M., Vitelli, V., Renaudin, X., Adamowicz, M., Iannelli, F., Jones-Weinert, C.W., Lee, M., Matti, V., et al. (2018). BRCA2 controls DNA:RNA hybrid level at DSBs by mediating RNase H2 recruitment. *Nat. Commun.* 9, 5376. <https://doi.org/10.1038/s41467-018-07799-2>.
4. Cohen, S., Puget, N., Lin, Y.-L., Clouaire, T., Aguirrebengoa, M., Rocher, V., Pasero, P., Canitrot, Y., and Legube, G. (2018). Senataxin resolves RNA:DNA hybrids forming at DNA double-strand breaks to prevent translocations. *Nat. Commun.* 9, 533. <https://doi.org/10.1038/s41467-018-02894-w>.
5. Tan, J., Duan, M., Yadav, T., Phoon, L., Wang, X., Zhang, J.-M., Zou, L., and Lan, L. (2020). An R-loop-initiated CSB-RAD52-POLD3 pathway suppresses ROS-induced telomeric DNA breaks. *Nucleic Acids Res.* 48, 1285–1300. <https://doi.org/10.1093/nar/gkz1114>.
6. Skourtis-Stathaki, K., Proudfoot, N.J., and Gromak, N. (2011). Human senataxin resolves RNA/DNA hybrids formed at transcriptional pause sites to promote Xrn2-dependent termination. *Mol. Cell* 42, 794–805. <https://doi.org/10.1016/j.molcel.2011.04.026>.
7. Sze, S., Bhardwaj, A., Fnu, P., Azarm, K., Mund, R., Ring, K., and Smith, S. (2023). TERRA R-loops connect and protect sister telomeres in mitosis. *Cell Rep.* 42, 113235. <https://doi.org/10.1016/j.celrep.2023.113235>.
8. Balk, B., Maicher, A., Dees, M., Klermund, J., Luke-Glaser, S., Bender, K., and Luke, B. (2013). Telomeric RNA-DNA hybrids affect telomere-length dynamics and senescence. *Nat. Struct. Mol. Biol.* 20, 1199–1205. <https://doi.org/10.1038/nsmb.2662>.
9. Arab, K., Karaivanov, E., Musheev, M., Trnka, P., Schäfer, A., Grummt, I., and Niehrs, C. (2019). GADD45A binds R-loops and recruits TET1 to CpG

- island promoters. *Nat. Genet.* 51, 217–223. <https://doi.org/10.1038/s41588-018-0306-6>.
10. Sun, Q., Csorba, T., Skourti-Stathaki, K., Proudfoot, N.J., and Dean, C. (2013). R-loop stabilization represses antisense transcription at the Arabidopsis FLC locus. *Science* 340, 619–621. <https://doi.org/10.1126/science.1234848>.
11. Sanz, L.A., Hartono, S.R., Lim, Y.W., Steyaert, S., Rajpurkar, A., Ginno, P.A., Xu, X., and Chédin, F. (2016). Prevalent, dynamic, and conserved R-loop structures associate with specific epigenomic signatures in mammals. *Mol. Cell* 63, 167–178. <https://doi.org/10.1016/j.molcel.2016.05.032>.
12. García-Muse, T., and Aguilera, A. (2019). R-Loops: From Physiological to Pathological Roles. *Cell* 179, 604–618. <https://doi.org/10.1016/j.cell.2019.08.055>.
13. Brickner, J.R., Garzon, J.L., and Cimprich, K.A. (2022). Walking a tightrope: The complex balancing act of R-loops in genome stability. *Mol. Cell* 82, 2267–2297. <https://doi.org/10.1016/j.molcel.2022.04.014>.
14. Petermann, E., Lan, L., and Zou, L. (2022). Sources, resolution and physiological relevance of R-loops and RNA-DNA hybrids. *Nat. Rev. Mol. Cell Biol.* 23, 521–540. <https://doi.org/10.1038/s41580-022-00474-x>.
15. Miglietta, G., Russo, M., and Capranico, G. (2020). G-quadruplex–R-loop interactions and the mechanism of anticancer G-quadruplex binders. *Nucleic Acids Res.* 48, 11942–11957. <https://doi.org/10.1093/nar/gkaa944>.
16. Freudenreich, C.H. (2018). R-loops: Targets for Nuclease Cleavage and Repeat Instability. *Curr. Genet.* 64, 789–794. <https://doi.org/10.1007/s00294-018-0806-z>.
17. Luna, R., Gómez-González, B., and Aguilera, A. (2024). RNA biogenesis and RNA metabolism factors as R-loop suppressors: a hidden role in genome integrity. *Genes Dev.* 38, 504–527. <https://doi.org/10.1101/gad.351853.124>.
18. Bonnet, A., Grosso, A.R., Elkaoutari, A., Coleno, E., Presle, A., Sridhara, S.C., Janbon, G., Géli, V., de Almeida, S.F., and Palancade, B. (2017). Introns Protect Eukaryotic Genomes from Transcription-Associated Genetic Instability. *Mol. Cell* 67, 608–621.e6. <https://doi.org/10.1016/j.molcel.2017.07.002>.
19. Cerritelli, S.M., and Crouch, R.J. (2009). Ribonuclease H: the enzymes in eukaryotes. *FEBS J.* 276, 1494–1505. <https://doi.org/10.1111/j.1742-4658.2009.06908.x>.
20. Costantino, L., and Koshland, D. (2018). Genome-wide Map of R-Loop-Induced Damage Reveals How a Subset of R-Loops Contributes to Genomic Instability. *Mol. Cell* 71, 487–497.e3. <https://doi.org/10.1016/j.molcel.2018.06.037>.
21. Mischo, H.E., Gómez-González, B., Grzechnik, P., Rondón, A.G., Wei, W., Steinmetz, L., Aguilera, A., and Proudfoot, N.J. (2011). Yeast Sen1 helicase protects the genome from transcription-associated instability. *Mol. Cell* 41, 21–32. <https://doi.org/10.1016/j.molcel.2010.12.007>.
22. Heuzé, J., Kemiha, S., Barthe, A., Vilarrubias, A.T., Aouadi, E., Aiello, U., Libri, D., Lin, Y.-L., Lengronne, A., Poli, J., and Pasero, P. (2023). RNase H2 degrades toxic RNA:DNA hybrids behind stalled forks to promote replication restart. *EMBO J.* 42, e113104. <https://doi.org/10.15252/embj.2022113104>.
23. San Martín-Alonso, M., Soler-Oliva, M.E., García-Rubio, M., García-Muse, T., and Aguilera, A. (2021). Harmful R-loops are prevented via different cell cycle-specific mechanisms. *Nat. Commun.* 12, 4451. <https://doi.org/10.1038/s41467-021-24737-x>.
24. Appanah, R., Lones, E.C., Aiello, U., Libri, D., and De Piccoli, G. (2020). Sen1 Is Recruited to Replication Forks via Ctf4 and Mrc1 and Promotes Genome Stability. *Cell Rep.* 30, 2094–2105.e9. <https://doi.org/10.1016/j.celrep.2020.01.087>.
25. Aiello, U., Challal, D., Wentzinger, G., Lengronne, A., Appanah, R., Pasero, P., Palancade, B., and Libri, D. (2022). Sen1 is a key regulator of transcription-driven conflicts. *Mol. Cell* 82, 2952–2966.e6. <https://doi.org/10.1016/j.molcel.2022.06.021>.
26. Arudchandran, A., Cerritelli, S., Narimatsu, S., Itaya, M., Shin, D.Y., Shimada, Y., and Crouch, R.J. (2000). The absence of ribonuclease H1 or H2 alters the sensitivity of *Saccharomyces cerevisiae* to hydroxyurea, caffeine and ethyl methanesulphonate: implications for roles of RNases H in DNA replication and repair. *Genes Cells* 5, 789–802. <https://doi.org/10.1046/j.1365-2443.2000.00373.x>.
27. Zimmer, A.D., and Koshland, D. (2016). Differential roles of the RNases H in preventing chromosome instability. *Proc. Natl. Acad. Sci. USA* 113, 12220–12225. <https://doi.org/10.1073/pnas.1613448113>.
28. Lockhart, A., Pires, V.B., Bento, F., Kellner, V., Luke-Glaser, S., Yakoub, G., Ulrich, H.D., and Luke, B. (2019). RNase H1 and H2 Are Differentially Regulated to Process RNA-DNA Hybrids. *Cell Rep.* 29, 2890–2900.e5. <https://doi.org/10.1016/j.celrep.2019.10.108>.
29. Roy, S., Adhikary, H., Isler, S., and D'Amours, D. (2024). The Smc5/6 complex counteracts R-loop formation at highly transcribed genes in cooperation with RNase H2. *eLife* 13, e96626. <https://doi.org/10.7554/eLife.96626>.
30. Heuzé, J., Kemiha, S., Barthe, A., Vilarrubias, A.T., Aouadi, E., Aiello, U., Libri, D., Lin, Y.-L., Lengronne, A., Poli, J., and Pasero, P. (2023). RNase H2 degrades toxic RNA:DNA hybrids behind stalled forks to promote replication restart. *EMBO J.* 42, e113104. <https://doi.org/10.15252/embj.2022113104>.
31. El Hage, A., French, S.L., Beyer, A.L., and Tollervey, D. (2010). Loss of Topoisomerase I leads to R-loop-mediated transcriptional blocks during ribosomal RNA synthesis. *Genes Dev.* 24, 1546–1558. <https://doi.org/10.1101/gad.573310>.
32. Amon, J.D., and Koshland, D. (2016). RNase H enables efficient repair of R-loop induced DNA damage. *eLife* 5, e20533. <https://doi.org/10.7554/eLife.20533>.
33. Steinmetz, E.J., Warren, C.L., Kuehner, J.N., Panbehi, B., Ansari, A.Z., and Brow, D.A. (2006). Genome-wide distribution of yeast RNA polymerase II and its control by Sen1 helicase. *Mol. Cell* 24, 735–746. <https://doi.org/10.1016/j.molcel.2006.10.023>.
34. Hazelbaker, D.Z., Marquardt, S., Wlotzka, W., and Buratowski, S. (2013). Kinetic competition between RNA Polymerase II and Sen1-dependent transcription termination. *Mol. Cell* 49, 55–66. <https://doi.org/10.1016/j.molcel.2012.10.014>.
35. Tudek, A., Porrua, O., Kabzinski, T., Lidschreiber, M., Kubicek, K., Fortova, A., Lacroute, F., Vanacova, S., Cramer, P., Stefl, R., and Libri, D. (2014). Molecular basis for coordinating transcription termination with noncoding RNA degradation. *Mol. Cell* 55, 467–481. <https://doi.org/10.1016/j.molcel.2014.05.031>.
36. Schulz, D., Schwalb, B., Kiesel, A., Baejen, C., Torkler, P., Gagneur, J., Soeding, J., and Cramer, P. (2013). Transcriptome surveillance by selective termination of noncoding RNA synthesis. *Cell* 155, 1075–1087. <https://doi.org/10.1016/j.cell.2013.10.024>.
37. Tsirkas, I., Dovrat, D., Thangaraj, M., Brouwer, I., Cohen, A., Paleiov, Z., Meijler, M.M., Lenstra, T., and Aharoni, A. (2022). Transcription-replication coordination revealed in single live cells. *Nucleic Acids Res.* 50, 2143–2156. <https://doi.org/10.1093/nar/gkac069>.
38. Varon, M., Dovrat, D., Heuzé, J., Tsirkas, I., Singh, S.P., Pasero, P., Galletto, R., and Aharoni, A. (2024). Rrm3 and Pif1 division of labor during replication through leading and lagging strand G-quadruplex. *Nucleic Acids Res.* 52, 1753–1762. <https://doi.org/10.1093/nar/gkad1205>.
39. Zardoni, L., Nardini, E., Brambati, A., Lucca, C., Choudhary, R., Loperfido, F., Sabbioneda, S., and Liberi, G. (2021). Elongating RNA polymerase II and RNA:DNA hybrids hinder fork progression and gene expression at sites of head-on replication-transcription collisions. *Nucleic Acids Res.* 49, 12769–12784. <https://doi.org/10.1093/nar/gkab1146>.
40. Tsirkas, I., Lee, C.S.K., Dovrat, D., Singh, N., Paleiov, Z., Lalonde, M., Sajid, A., Aharoni, A., and Hamperl, S. (2025). Replisome progression regulates R-loop mediated transcriptional repression. Preprint at bioRxiv. <https://doi.org/10.1101/2025.07.29.667376>.

41. Wahba, L., Amon, J.D., Koshland, D., and Vuica-Ross, M. (2011). RNase H and multiple RNA biogenesis factors cooperate to prevent RNA:DNA hybrids from generating genome instability. *Mol. Cell* 44, 978–988. <https://doi.org/10.1016/j.molcel.2011.10.017>.
42. Morawska, M., and Ulrich, H.D. (2013). An expanded tool kit for the auxin-inducible degron system in budding yeast. *Yeast* 30, 341–351. <https://doi.org/10.1002/yea.2967>.
43. Soreanu, I., Hendler, A., Dahan, D., Dovrat, D., and Aharoni, A. (2018). Marker-free genetic manipulations in yeast using CRISPR/CAS9 system. *Curr. Genet.* 64, 1129–1139. <https://doi.org/10.1007/s00294-018-0831-y>.
44. Quintero, M.J., Maya, D., Arévalo-Rodríguez, M., Cebolla, A., and Chávez, S. (2007). An improved system for estradiol-dependent regulation of gene expression in yeast. *Microb. Cell Fact.* 6, 10. <https://doi.org/10.1186/1475-2859-6-10>.

STAR★METHODS

KEY RESOURCES TABLE

REAGENT or RESOURCE	SOURCE	IDENTIFIER
Antibodies		
Rabbit monoclonal anti-alpha Tubulin antibody [EPR13799]	Abcam	Cat# ab184970; RRID:AB_2928998
Rat monoclonal anti-HA High Affinity (clone 3F10)	Roche	Cat# ROAHAHA; RRID: AB_2687407
Mouse monoclonal anti-HA (clone 12CA5)	Roche	Cat# 11666606001; RRID: AB_514506
Rabbit polyclonal anti-Histone H3	Abcam	Cat# ab1791; RRID: AB_302613
Mouse monoclonal anti-Phosphoglycerate Kinase 1 (22C5D8; Pgk1)	Invitrogen	Cat# 459250; RRID: AB_2532235
Goat Immun-Star anti-mouse (GAM)-HRP conjugate	Bio-Rad	Cat# 170-5047; RRID: AB_11125753
Goat polyclonal anti-Mouse-IRDye 800CW	Li-COR	Cat# 926-32210; RRID: AB_621842
Mouse monoclonal anti-c-Myc (Clone 9E10)	Sigma-Aldrich	Cat# MABE282; RRID: AB_11213164
Goat Immun-Star anti-rabbit (GAR)-HRP conjugate	Bio-Rad	Cat# 170-5046; RRID: AB_11125757
Goat polyclonal anti-Rabbit-IRDye 680RD	Li-COR	Cat# 926-68071; RRID: AB_10956166
Mouse monoclonal anti-Rad53 (EL7.E1)	Abcam	Cat# ab166859; RRID: AB_2801547
Monoclonal ANTI-FLAG® M2-Peroxidase (HRP) antibody	Sigma-Aldrich	Cat# A8592, RRID:AB_439702
Rabbit polyclonal anti-Ribonucleoside-diphosphate reductase large chain 2 (Rnr3)	Agrisera Antibodies	Cat# AS09 574; RRID: AB_1966947
Mouse monoclonal anti-DNA-RNA Hybrid (S9.6)	Kerafast	Cat# ENH001; RRID: AB_2687463
Mouse monoclonal anti-dsDNA	Abcam	Cat# ab27156; RRID: AB_470907
Chemicals, peptides, and recombinant proteins		
2-mercaptoethanol	Sigma-Aldrich	Cat#M6250
Ambion™ RNase III	Thermo Fisher Scientific	Cat#AM2290
Alpha factor mating pheromone	Zymo Research	Cat#Y1001
Benzonase® Nuclease	Sigma-Aldrich	Cat#E1014
15 mL Bioruptor® Pico Tubes & sonication beads	Diagenode	Cat#C01020031
Bovine serum albumin	Sigma-Aldrich	Cat#A4919-100G
Complete™ Mini EDTA-free protease inhibitor cocktail tablets	Roche	Cat#4693159001
ddPCR™ Droplet Reader Oil	BioRad	Cat#1863004
Deoxyribonucleotides (dNTPs, 10 mM each)	Invitrogen	Cat#N0447L
Dynabeads™ Protein G	Invitrogen	Cat#10607605
Formaldehyde 37%	Sigma Aldrich	Cat#F8775-500ML
Hydroxyurea	Sigma-Aldrich	Cat#H8627-25G
Lysis Matrix C tubes	MP Biomedicals	Cat#1169120-CF
Methyl methanesulfonate	Sigma-Aldrich	Cat#129925-25G
4–15% Mini-PROTEAN™ TGX Stain-Free™ Protein Gels, 15 well	Bio-Rad	Cat#4568086
4–15% Mini-PROTEAN™ TGX Stain-Free™ Protein Gels, 10 well	Bio-Rad	Cat#4568083
7.5% Mini-PROTEAN™ TGX Stain-Free™ Protein Gels, 15 well	Bio-Rad	Cat#4568026
7.5% Mini-PROTEAN™ TGX Stain-Free™ Protein Gels, 10 well	Bio-Rad	Cat#4568023
Nonidet P40 (NP40)	AppliChem	Cat#A1694,0500
Phenol equilibrated, stabilized: Chloroform:	AppliChem	Cat#A0889,0500
Isoamyl Alcohol 25 : 24: 1		

(Continued on next page)

Continued

REAGENT or RESOURCE	SOURCE	IDENTIFIER
PhosSTOP	Roche	Cat#04906845001
Proteinase K	BioFroxx	Cat#1151ML010
Q5 HotStart High-Fidelity DNA Polymerase	New England Biolabs	Cat#M0493L
QX200TM ddPCRTM EvaGreen Supermix	Bio-Rad	Cat#186-4033
Random hexamers	Thermo Fisher Scientific	Cat#SO142
RNase A	Thermo Fisher Scientific	Cat#EN0531
RNase H	New England Biolabs	Cat#M0297L
RNase T1	Thermo Fisher Scientific	Cat#EN0542
RNaseOutTM	Invitrogen	Cat#10777019
Superfrost TM Plus Adhesion Microscope Slides	Epredia	Cat#10149870
SuperScript TM III Reverse Transcriptase	Invitrogen	Cat#18080044
SuperSignal TM West FEMTO Chemiluminescent Substrate	Thermo Fisher Scientific	Cat#34094
SuperSignal TM West Pico PLUS chemiluminescent substrate	Thermo Fisher Scientific	Cat#15669364
SYTOX Green nucleic acid stain	Thermo Fisher Scientific	Cat#S7020
Zymolyase® 20T (<i>Arthrobacter luteus</i>)	Amsbio	Cat#120491-1
Critical commercial assays		
Gentra Puregene Yeast/Bact. Extraction Kit B	Qiagen	Cat#158567
QIAquick PCR purification kit	Qiagen	Cat#28106
riboPool kit	siTOOLs	Cat#dp-P024-5
RNase-Free DNase Set	Qiagen	Cat#79254
TruSeq stranded Total RNA LT Sample Prep Kit	Illumina	Cat#20020598
Deposited data		
RNA sequencing	This study	SRA: PRJNA1212884
Experimental models: Organisms/strains		
<i>S. cerevisiae</i> strains, S288C background derivatives	This study	See Table S1
Oligonucleotides		
Primers	This study	See Table S2
Software and algorithms		
CFX manager 3.1	Bio-Rad	http://www.bio-rad.com/de-de/sku/1845000-cfx-manager-software ; RRID: SCR_018057
Fiji 1.51d (ImageJ)	NIH	https://imagej.net/software/fiji/ ; RRID: SCR_002285
FlowJo 10.10	BD Life Sciences	https://www.flowjo.com/ ; RRID: SCR_008520
GraphPad Prism 10.4.1	GraphPad	https://www.graphpad.com/scientific-software/prism/ ; RRID: SCR_002798
Illustrator 27.8	Adobe	http://www.adobe.com/products/illustrator.html ; RRID: SCR_010279
Image lab 6.1	Bio-Rad	https://www.bio-rad.com/de-de/product/image-lab-software ; RRID: SCR_014210
Image studio 3.1	Li-COR	https://www.licor.com/bio/image-studio/ ; RRID:SCR_015795
Quantasoft TM Analysis Pro	Bio-Rad	https://commerce.bio-rad.com/webroot/web/software/lsr/Downloads/AmplificationPCR/quantasoftAP_1.0.596_Setup.zip?_gl=1*jciqv0*_gcl_au*R0NMLjE3NDI1NDkzNzMuRUFJYUIRb2JDaE1Jek1ldG1PNmFqQU1WQ1pLREJ4M21BUjVaRUFBUFTQUFFZ0l6aWZEX0J3RQ.*_gcl_au*MTA0OTM3NDE5MC4xNzMTgZgMjYx ; RRID:SCR_025321
R	The R Foundation	https://www.r-project.org/ ; RRID: SCR_001905

(Continued on next page)

Continued

REAGENT or RESOURCE	SOURCE	IDENTIFIER
Seaborn	Michael Waskom	https://seaborn.pydata.org/ ; RRID:SCR_018132
Zen Microscopy Software 3.0	Zeiss	https://www.zeiss.com/microscopy/en/products/software/zeiss-zen.html ; RRID:SCR_013672
Other		
Bio-Dot® SF Filter paper	Bio-Rad	Cat#1620161
DG8TM Cartridges for QX200TM Droplet Generator	Bio-Rad	Cat#1864008
DG8TM Gaskets for QX200TM Droplet Generator	Bio-Rad	Cat#1863009
Dotblot apparatus 'Bio-Dot'	Bio-Rad	Cat#1706545
Microseal® 'B' PCR Plate Sealing Film	Bio-Rad	Cat#17010701
Nylon Membrane, positively charged	Roche	Cat#11417240001

EXPERIMENTAL MODEL AND STUDY PARTICIPANT DETAILS

Saccharomyces cerevisiae strains used in this paper are derivatives of the standard strain S288C and are listed in Table S1.

Strains were grown under standard conditions in YPD (Yeast Peptone Dextrose) or SC without amino acids (Synthetic Complete) at 30°C if not indicated otherwise. Further specifications are mentioned within the method details and Figure legends section.

METHOD DETAILS

Yeast strain generation

AID*-tagged strains were constructed as described previously.⁴² Yeast knock out strains were taken from yeast knock out collections.^{18–20} For microscopy measurements (Figures 5C and 5D), strains were generated as previously described³⁷ with minor modifications. Briefly, strains for replication measurements were generated on a W1588 *MATa* background, where LacI-HaloTag and TetR-tdTomato fusion proteins are expressed for nuclear localization.^{37,38} Non-repetitive *lacOx128* and *tetOx160* arrays were then integrated using a CRISPR-Cas9 marker-free approach⁴³ at the vicinity of *ARS413* at chrIV:332960 and chrIV:352560, respectively, with an inter-array distance of ~25.5 kb. Subsequently, the mAIRN gene was integrated in co-directional orientation between the *lacO* and *tetO* arrays in chrIV:336187 using the CRISPR approach.⁴³ Sen1-AID was fused to the AID* tag by genomic integration marked with *hphMX* antibiotic resistance cassette.⁴² A GEM plasmid for the expression of estradiol receptor-Gal4-transcription activation domain (provided by the Pasero lab) was linearized and integrated into the *AUR1* locus for the estradiol-mediated induction of mAIRN.⁴⁴ To enable the auxin (IAA) induced depletion of Sen1-AID, *TIR1* gene from *Oryza sativa* was integrated at the *ADE1* locus.

Cell-cycle arrest and release

For arresting cells in G1, cells carrying mating type “a” were treated with 2.4 μM alpha factor for 1.5 h–2 h. The cells were either kept in G1 for further experiments or the alpha factor was washed out for releasing them to the cell cycle. For the release, the cells were spun down for 3 min at 900 x g and RT and the supernatant was discarded. The cells were washed three times in one culture volume sterile ddH₂O and spun down again like before. The cells were resuspended in the same volume of YPD or suitable drop out medium (pre-warmed to 25°C) as the initial culture volume. The release was performed at 25°C in the water bath shaker.

Western blot

Protein extraction was carried out by Trichloroacetic acid (TCA) extraction. First, 2 OD₆₀₀ units of pelleted yeast cells were resuspended in 140 μL 1.85 N NaOH containing 7.6% beta-Mercaptoethanol and incubated for 10 min on ice. 140 μL 50% Trichloroacetic acid were added and the samples were mixed well. After incubating again for 10 min on ice, the samples were spun down at 18000 x g and 4°C for 2 min. The supernatant was removed and the pellet was washed in 1 mL ice-cold Acetone. The samples were spun down at 18000 x g and 4°C for 2 min 100 μL urea buffer (120 mM Tris-HCl pH 6.8, 5% (v/v) Glycerol, 8 M Urea, 143 mM beta-Mercaptoethanol, 8% (v/v) SDS and Bromphenol blue) was added to the samples, followed by incubation at 95°C for 3 min.

For the SDS-PAGE, precast acrylamide gels from the BioRad Mini-PROTEAN TGX Stain-Free system were used. For the protein transfer to membranes, the BioRad Trans-Blot Turbo Transfer System was used.

The following antibodies were used for immunostaining:

Primary antibodies: α-Pgk1 (Invitrogen) at 1:20000; α-H3 (Abcam) at 1:1000. Anti-HA (Clone 12CA5) at 1:3000, anti-Myc (Clone 9E10) at 1:1000, anti-γH2A (pS129; Abcam) at 1:1000, Anti-α-Tubulin (Abcam) at 1:20000, anti-Rad53 (Abcam) 1:1000, anti-Rnr3 (Agrisera Antibodies) 1:1000, anti-FLAG antibody conjugated to HRP enzyme (Sigma-Aldrich) 1:1000.

Secondary antibodies: Goat anti-rabbit -HRP conjugate, (Bio-Rad) at 1:3000 Goat anti-mouse -HRP conjugate (Bio-Rad) at 1:3000, IRDye 680RD Goat anti-Rabbit (Li-Cor) at 1:2000 or IRDye 800CW Goat anti-Mouse (Li-Cor) at 1:2000.

Proteins were detected using the Super Signal West Pico Chemiluminescent Substrate (Thermo Scientific) on Bio-Rad ChemiDoc Touch Imaging System or on the Li-Cor Odyssey XF imaging system.

DNA content flow cytometry

0.18 OD₆₀₀ units exponentially cycling cells were spun down at 900 x g at RT. The cells were washed in 1 mL ddH₂O and spun down as before. The cells were resuspended in 70% EtOH and stored at 4°C overnight.

The samples were spun at 16200 x g and RT for 5 min. The pellet was resuspended in 1 mL 50 mM Tris-HCl (pH 7.4) and the centrifugation was repeated. The cells were resuspended in 500 µL 0.25 mg/mL RNase A (Thermo Scientific) and incubated at 37°C for 3 h or overnight. 25 µL 20 mg/mL Proteinase K solution (Biofrox) were added and the samples were incubated for 2 h at 50°C. The samples were sonicated using a Branson Sonifier (10 s, constant mode, 10% power). 500 µL 4 µM Sytox green in 50 mM Tris-HCl (pH 7.4) were added and the samples were measured using the BD FACS Fortessa or Agilent Novocyte Quanteon flow cytometer. The analysis was carried out using the software “FlowJo”.

RNA extraction

For RNA extraction, 15 mL exponentially growing cells were collected and spun down for 3 min and 600 x g at RT. The Pellet was washed in 1 mL ddH₂O and the supernatant was removed very thoroughly.

The cell pellets were resuspended in 400 µL AE buffer (50 mM Sodium Acetate pH 5.3, 10 mM EDTA). 20 µL 20% SDS were added and the samples were vortexed. 500 µL phenol pre-equilibrated in AE-buffer were added and the samples were again vortexed. After 5 min incubation at 65°C and 5 min incubation on ice, the samples were spun down for 2 min at 20800 x g and 4°C. The aqueous phase was mixed with 500 µL Phenol: Chloroform: Isoamylalcohol (25 : 24: 1; AppliChem) were added by inverting 5 times. The samples were incubated for 5 min at RT, followed by spinning for 2 min at 20800 x g and 4°C. The aqueous phase was mixed with 40 µL 3 M Sodium acetate and 1 mL ice-cold 100% EtOH. The samples were inverted 5 times and incubated on ice for 15 min, followed by centrifugation for 2 min at 20800 x g and 4°C. The pellet was washed in 1 mL 80% EtOH and spun down for 2 min at 20800 x g and 4°C. The pellet was dried for 5 min and resuspended in 100 µL RDD buffer (Qiagen) with 4 µL DNase I (Qiagen). The samples were incubated at 37°C and 350 rpm for 30 min.

Reverse transcription

For reverse transcription, 1 µg RNA was preincubated with 1 µL NTPs (Invitrogen, 10 mM each) and 2 µL random primers (Thermo Scientific, 0.2 mM) in 13 µL ddH₂O for 5 min at 65°C. 4 µL 5x First Strand buffer (Invitrogen), 1 µL 0.1 M DTT (Invitrogen), 1 µL RNaseOut (Invitrogen) and 1 µL Superscript III (Invitrogen) were added to the samples. The samples were incubated for 5 min at 25°C, followed by 1 h at 50°C and 15 min at 75°C.

Digital droplet PCR

Exponentially growing yeast cells were counted using the Cellometer X1 (Nexcelom) and the count was adjusted manually to account for clumping yeast and particles identified as yeast. The RNA was extracted like described under “RNA extraction” and reverse transcribed like described under “reverse transcription”.

For the ddPCR, 1 µL cDNA was diluted to 12.5 µL in DPEC treated water containing 500 nM of each PCR primer. The samples were supplemented with 12.5 µL QX200 ddPCR EvaGreen Supermix (Bio-Rad) prior to droplet generation. For droplet generation, 20 µL of the sample and 70 µL droplet generator oil for EvaGreen (Bio-Rad) were loaded into a DG8 cartridge (Bio-Rad), covered by a DG8 gasket (Bio-Rad) and the droplets were generated using the QX200 droplet generator machine (Bio-Rad). 40 µL of the generated droplet were transferred into a 96 well plate (BioRad) and the plate was sealed using the PX1 PCR plate sealer (Bio-Rad) and PCR plate heat seal foil (Bio-Rad). The PCR was carried out using the following program: 5 min at 95°C, 40 cycles of 30 s at 95°C and 1 min at 60°C, 5 min at 4°C, 5 min at 95°C, 4°C until droplet read.

For the droplet read, the PCR plate was moved into the QX200 droplet reader (Bio-Rad) and the droplets were analyzed. The QuantaSoft analysis pro software (Bio-Rad) gives out transcripts per sample which can be used for calculating the transcripts per cell considering the cell count from the beginning.

RNA-seq

For RNA sequencing, 20 mL exponentially growing cells were collected by centrifugation for 3 min at 600 x g. The RNA was extracted and DNase I digested like described under “RNA extraction”. rRNA depletion was performed with a starting amount of 1500 ng using the riboPool kit from siTOOLS following riboPoolKitManual_v1-4 (December 2021). The RNA clean-up was performed with a ratio of 1.8x of RNA Clean XP beads to RNA volume. Library preparation was performed with Illumina TruSeq stranded Total RNA LT Sample Prep Kit following TruSeq Stranded total RNA Reference Guide (Oct.2017) (Document # 1000000040499v00) starting at the Fragmentation step. Libraries were amplified in 9 PCR cycles. Libraries were profiled in a High Sensitivity DNA on a 2100 Bioanalyzer

(Agilent technologies) and quantified using the Qubit dsDNA HS Assay Kit, in a Qubit 2.0 Fluorometer (Life technologies). All samples were pooled together in equimolar ratio and sequenced on a NextSeq 500 Midoutput flow cell, single read for 1x 75 cycles plus 8 + 8 bp cycles for the dual index read.

RT-qPCR

For RT-qPCR, the reverse transcribed RNA from “reverse transcription” was used. The cDNA was diluted to 50 μ L. As a no RT control, also 1 μ g untreated RNA was diluted in 50 μ L ddH₂O. The PCR was carried out in 384 well plates using the CFX Real-time PCR cycler with 384 well add-in from BioRad. The reaction volume was 10 μ L, consisting of 4 μ L cDNA or not reverse transcribed RNA, 0.9 μ L DPEC treated H₂O, 0.05 μ L of each primer (100 μ M stock) and 5 μ L Eva green Master Mix. The PCR plate was sealed using Microseal ‘B’ PCR Plate Sealing Film and the spun down shortly. The PCR program was the following: 10 min at 95°C, followed by 40 cycles of 15 s at 95°C and 1 min at 60°C. Afterward melting curves were measures from 65.0°C until 96.5°C in 0.5°C steps. The qPCR results were analyzed using the Bio-Rad RFX Manager software. The c_q determination method was set to “regression” and the data was exported. The further analysis was carried out in Excel. The mean of the technical replicates was calculated and the actin (house-keeping gene) values were subtracted. The following formula was used for the calculation:

$$\text{Transcript level normalized to actin} = 2^{-(c_{q,\text{transcript of interest}} - c_{q,\text{actin}})}$$

3'RACE

The cultures were grown to OD₆₀₀ 0.4 and 10 mL of the culture were collected. The cells were spun down for 3 min at 900 x g and RNA was extracted like described under “RNA extraction”. The RNA was reverse transcribed like described under “reverse transcription” using a 3'RACE specific primer (oCW128; poly-T primer carrying an adaptor sequence from Mischo et al., 2011). The resulting cDNA was used in a with a gene specific primer in combination with the reverse adaptor primer (oCW129 from Mischo et al., 2011). The PCR was setup in 25 μ L total volume, using 1 μ L cDNA, both primers at 10 μ M and 2x Q5 Master Mix (NEB) in the following program: 30 s at 98°C, 35 cycles of (5 s at 98°C, 15 s at 66°C and 20 s at 72°C) and final elongation for 2 min at 72°C. The samples were analyzed on a 2% agarose gel, run at 100 V for 1 h. The gels were imaged using the Bio-Rad ChemiDoc Touch Imaging System.

Chromatin immunoprecipitation

Chromatin immunoprecipitation (ChIP) experiments were in general conducted like described in our published method for R-ChIP.²¹ In brief, 150 mL exponentially growing cell cultures were diluted to OD₆₀₀ 0.6 in 150 mL. For crosslinking, 4.9 mL 37% Formaldehyde (0.84% final) were added and the cultures were incubated for 10 min at RT. The crosslinking was quenched by adding 7.5 mL 2.5 M Glycine for 5 min at RT, followed by 5 min on ice. The cells were precipitated by centrifugation at 4°C and 3000 x g for 3 min. The cell pellets were washed twice in 20 mL ice-cold 1x PBS. The dry cell pellets were stored at –80°C until further processing.

For immunoprecipitation, each sample was resuspended in 200 μ L FA lysis buffer minus SOD (50 mM HEPES-KOH pH 7.5, 140 mM NaCl, 1 mM EDTA, 1% (v/v) Triton X-100, 1 protease inhibitor tablet per 10 mL buffer (Roche)) and transferred to an lysing matrix C tube. The cell lysis was carried out using the FastPrep (MP Biomedicals) machine at the speed of 6 m/s for 30 s twice, placing the samples on ice in between for 1 min. For recovery, 800 μ L of the FA lysis buffer plus SOD (50 mM HEPES-KOH pH 7.5, 140 mM NaCl, 1 mM EDTA, 1% (v/v) Triton X-100, 0.1% (w/v) Sodium deoxycholate, one protease inhibitor tablet per 10 mL buffer (Roche)) was added and the mixture was transferred to a fresh 2 mL centrifugation tube. The samples were centrifuged at 17000 x g and 4°C for 7 min. The supernatant was discarded and the pellet was resuspended in 1.5 mL FA lysis buffer plus SOD and 20 μ L of 20% SDS. The samples were transferred into 15 mL sonication tubes containing 0.8 g–1.0 g sonication beads. The sonication was carried out twice in 10 cycles (30 s on, 30 s off) with a 15 min break on ice in between using a Bioruptor pico (Diagenode).

In the meantime, the magnetic beads were prepared. Per samples, 200 μ L Dynabeads Protein G (Thermo Fisher Scientific) 10 mL 1x PBS were added and the volume was adjusted to 6 mL for blocking with 5% molecular biology grade BSA (final, w/v, NEB). The beads were incubated for 1 h on a rotating wheel at 4°C. The beads were washed in 10 mL 1x PBS, followed by a wash in 10 mL FA lysis buffer plus SOD. The supernatant was removed for reaching the initial filling volume of the beads.

The sonified samples were centrifuged at 17000 x g and 4°C for 15 min. The supernatant was collected and is called ChIP extract. The protein concentration of the ChIP extract was measured using a Bradford assay. The samples were diluted to 1 mg/mL in 2.2 mL FA lysis buffer plus SOD with protease inhibitor. The samples were split in four fresh tubes.

- (1) 1 mL for immunoprecipitation.
- (2) 1 mL as immunoprecipitation negative control (no antibody).
- (3) 50 μ L as input sample (stored at –20°C).
- (4) 100 μ L for sonication control.

The sonication control samples were mixed with 100 mL Elution buffer B (50 mM Tris-HCl pH 7.5, 1% SDS, 10 mM EDTA pH 8), supplemented with 7.5 μ L Proteinase K (20 mg/mL) and incubated overnight shaking at 450 rpm and 65°C. The samples were EtOH

precipitated by adding 1 mL 100% EtOH and incubating 20 min at -80°C , followed by centrifugation for 15 min $20000 \times g$ at 4°C . The samples were resuspended in 20 μL ddH₂O and were supplemented with 1 μL RNase A (10 mg/mL). After incubating for 30 min at 37°C , the sonication was verified on an agarose gel.

The immunoprecipitation samples were precleared by adding 30 μL of the prepared magnetic beads and incubation for 1 h on a rotating wheel at 4°C . The supernatant was transferred to a fresh tube. For the negative control samples, no antibody was added, while to the immunoprecipitation samples antibody was added (10 μL Anti-HA 3F10 (Roche) for R-ChIP or 4 μL S9.6 (Kerafast) for DRIP). The samples were incubated for 30 min on a rotating wheel at 4°C . 50 μL of the prepared magnetic beads were added and the samples were incubated overnight on a rotating wheel at 4°C .

The IP samples were washed in four steps, using 1 mL of each of the following buffers and incubating for 5 min at 4°C on a rotating wheel: 1. FA cell lysis buffer plus SOD 2. FA 500/lysis buffer (50 mM HEPES-KOH pH 7.5, 500 mM NaCl, 1 mM EDTA, 1% (v/v) Triton X-100, 0.1% (w/v) Sodium deoxycholate), 3. Buffer III (10 mM Tris-HCl pH 8.0, 1 mM EDTA, 250 mM LiCl, 1% (v/v) Tergitol-type NP-40, 1% (w/v) sodium deoxycholate), 4. 1x TE buffer.

After the last wash, the magnetic beads were resuspended in 100 μL Elution buffer B immediately. At this point, the input samples were thawed and supplemented with 150 μL Elution buffer B. For the elution, the input samples and the IP samples were incubated together. The elution was carried out for 8 min at 65°C and 850 rpm on a heat block. The supernatant was transferred to a fresh tube. 100 μL of fresh Elution buffer B were added and the elution was repeated. After pooling the eluents, 7.5 μL Proteinase K (20 mg/mL) were added to the IP and input samples. The samples were incubated overnight at 65°C , shaking at 450 rpm on a heat block.

The samples were purified using the Qiagen PCR purification kit, eluting the DNA with 50 μL DPEC treated water. The quantitative real-time PCR was prepared in a 384 well PCR plate. The reaction mix per well was the following in 10 μL total volume: 1 μL DNA, 5 μM of each primer, 5 μL of Eva green qPCR Master mix. The PCR was carried out under the following conditions: 10 min at 95°C , 40 cycles of 15 s at 95°C and 1 min at 60°C , followed by a melting curve measurement (65.0°C till 96.5°C in 0.5°C steps).

The analysis of the data was carried out using the Bio-Rad CFX Manager software. The data was imported, the C_q determination method was set to "regression" and the data was exported to Excel. The mean C_q of the technical replicates was calculated and the C_q value of the input sample was corrected to account for the 1:20 dilution compared to the IP samples:

$$\log_2(20) = 4.322,$$

$$C_q(\text{corr. input}) = C_q(\text{input}) - 4.322.$$

The percent input of the IP samples was calculated:

$$\Delta C_q = C_q(\text{corr. input}) - C_q(\text{sample} \pm \text{antibody}),$$

$$\text{Percent input} = 100 * 2^{\Delta C_q}.$$

Spotting assay

Overnight cultures of budding yeast were diluted in 10-fold serial dilution in sterile ddH₂O, starting from OD₆₀₀ 0.5. The yeast dilutions were spotted onto agar plates using a replica plater stamp. The plates were incubated at 30°C if not indicated differently. Images of the plates were taken after 24 h, 48 h and 72 h using the Bio-Rad ChemiDoc Touch Imaging System (Colorimetric mode, 0.3 s exposure).

CHX chase assay

In order to start the Cycloheximide (CHX) chase assay, an untreated sample was taken as 0 min time point. The collected OD₆₀₀ units were dependent on the chosen analysis method (simple Western blot: 2 OD₆₀₀; Chromatin binding assay: at least 12 OD₆₀₀). The cell culture were either treated with 200 $\mu\text{g}/\text{mL}$ CHX or stayed untreated. Samples were collected adding the collected volume to a sufficient amount of 10% NaAz in order to reach 0.1% NaAz (end concentration) on ice. The volume was corrected in order to reach the right amount of OD₆₀₀ units. The samples were spun down for 3 min at $600 \times g$ at RT and the supernatant was discarded. The samples were transferred to micro centrifugation tubes and stored at -20°C until further processing. The protein stability was determined by Western blot.

Chromatin binding assay

At least 12 OD of exponentially cycling cells were collected and spun down at $600 \times g$ at RT. The supernatant was discarded, the pellets were resuspended in 1 mL ddH₂O and transferred to fresh microcentrifugation tubes. The samples were again spun down at $900 \times g$ at RT and the dry pellets were stored at -20°C until further processing. The pellets were thawed on ice and resuspended in 1 mL spheroblasting buffer (50 mM phosphate buffer pH 7.4, 1 M Sorbitol, 1 mM DTT). The OD of the suspension was measured. 12 OD were diluted in 1 mL spheroblasting buffer. 5 μL Zymolyase T20 and 1 μL 1 M DTT were added and the samples were incubated at 30°C for 40 min. The cells were spun down at $400 \times g$ for 2 min and the supernatant was removed. The pelleted cells were

resuspended in 300 μ L extraction buffer (50 mM Tris-HCl pH 7.5, 100 mM KCl, 2.5 mM $MgCl_2$, 1 tablet per 10 mL proteinase inhibitor cocktail (Roche), 1 tablet per 10 mL PhosphoStop (Roche)).

- (1) 50 μ L for whole cell extract.
- (2) 50 μ L for soluble fraction.
- (3) 200 μ L for chromatin bound fraction.

The different fractions were treated in different ways.

- (1) Whole cell extract: 1.25 μ L 10% Triton-100 were added, the samples were quickly vortexed and incubated for 5 min on ice. 125 U/ μ L Benzonase was added, followed by 15 min incubation on ice. 20 μ L urea buffer were added and the samples were boiled at 75°C for 5 min.
- (2) Soluble fraction: 1.25 μ L 10% Triton-100 were added, the samples were quickly vortexed and incubated for 5 min on ice. The samples were spun for 10 min at 20000 xg and 4°C. 50 μ L of the supernatant were transferred to a fresh tube, 20 μ L urea buffer were added and the samples were boiled at 75°C for 5 min.
- (3) Chromatin bound fraction: 5 μ L 10% Triton-100 were added, the samples were quickly vortexed and incubated for 5 min on ice. 1 mL 30% ice-cold sucrose was added into fresh tubes and the samples were layered on top. The samples were spun for 10 min at 20000 xg and 4°C. The supernatant was removed and the pellets were resuspended in 200 μ L extraction buffer and 5 μ L 10% Triton-100. The sucrose step was repeated. The supernatant was removed and the pellet was resuspended in 50 μ L extraction buffer and 1.25 μ L 10% Triton-100. 125 U/ μ L Benzonase was added and the samples were incubated on ice for 15 min. 20 μ L urea buffer were added and the samples were boiled at 75°C for 5 min.

The samples were loaded to a precast 4 to 15% gradient polyacrylamide gel (Bio-Rad) and run at 140 V for 51 min.

Dotblot for measuring RNA:DNA hybrid levels

gDNA was extracted from exponentially growing yeast cells using the Gentra Puregene Yeast/Bact. Extraction Kit B (Qiagen) according to the manufacturers protocol, skipping the RNase A treatment step. The DNA pellet is dissolved in RNase-free water over night at 4°C. 4.8 μ g of the extracted gDNA was digested with an RNase cocktail in 100 μ L 1x RNase H buffer from NEB. The mixture contained the following RNases: 5 units RNase III (Thermo Fisher Scientific) and 1 unit RNase T1 (Thermo Fisher Scientific). The control samples contained additional 10 units RNase H (NEB). The digest was incubated for 3 h at 37°C, followed by heat inactivation for 20 min at 65°C. The samples were split in two and diluted to 240 μ L in 1x SSC buffer. In a 96-well plate, the initial was diluted in a 1:2 serial dilution in four steps, aiming for 120 μ L sample per well. 100 μ L of each sample and dilution was spotted onto a positively charged nylon membrane pre-soaked in 1x SSC, stacked on Bio-Dot SF Filter paper using a Dotblot apparatus (Bio-Rad). This creates spots with 2 μ g, 1 μ g, 0.5 μ g, 0.25 μ g and 1.25 μ g of DNA. The liquid was removed using a vacuum pump. The spotting process is repeated with the second sample, creating one membrane for the S9.6 signal and one for the loading control which is used for quantifying the dsDNA signal. The DNA is crosslinked to the membrane using a UVP crosslinker (Analytik Jena) with 120 mJ/cm². The membranes were blocked for 1 h at room temperature in 5% skim milk in 1x PBS +0.1% Tween 20. Both membranes are stained using different primary antibodies. For the first membrane 2 μ L of mouse S9.6 (Kerafast) in 10 mL 3% BSA were used and for the second membrane 10 μ L mouse anti-dsDNA (Abcam) in 10 mL 5% skim milk in 1x PBS +0.1% Tween 20 were used. The membranes were incubated overnight shaking at 4°C. The membranes were washed four times for 15 min in 1x PBS +0.1% Tween 20. Both blots were stained with the same secondary antibody which was 1:3000 goat anti-mouse-HRP (Bio-Rad). Which was incubated for 1 h at RT, followed by three washes for 15 min in 1x PBS +0.1% Tween 20 and one wash for 15 min in 1x PBS. The blots were developed on a Bio-Rad ChemiDoc System.

For quantification of the blots, ImageJ was used. In the software, the image was inverted and with the oval selection tool a circle was drawn around the spots that were chosen for quantification and the intensity was measured. Additionally, for subtracting the background, 5 circles that were distributed over the membrane were measured. The S9.6 signal was normalized to the dsDNA signal.

Microscopy

Microscopy experiments for replication measurements were performed as previously described^{37,38} with minor modifications. Briefly, yeast cells were grown overnight at 30°C in synthetic complete (SC) media supplemented with 4% glucose. Cultures were diluted to an OD₆₀₀ of 0.2, and SiR-HALO dye was added to reach 800 nM concentration. A 10 μ g/mL of α -factor (GenScript) was added for G1 arrest, followed by the addition of 500 nM of Estradiol (Sigma-Aldrich) to induce mAIRN expression, for an additional incubation of 2 h. For the uninduced cells, cultures were synchronized without the addition of estradiol. For Sen1-AID degradation, 1 mM of IAA (Thermo Fisher) was added 1 h before imaging. For microscopy, cells were immobilized on a precoated concanavalin A (Sigma) slide chamber (Ibidi) and washed to remove the α -factor and SiR-HALO dye. Live-cell imaging of the cells was performed on an Axio Observer microscope (Zeiss) as previously described.^{37,38}

QUANTIFICATION OF MICROSCOPY EXPERIMENTS AND STATISTICAL ANALYSIS

The imaging data was collected using ZEN 3.0 software and analyzed using AutoCRAT, which is a custom Python-based computational pipeline to measure replication times. Cells were analyzed and merged across 3–5 independent experiments for each strain and condition. Replication time data was statistically analyzed using Monte Carlo resampling with 1,000,000 iterations. To visualize replication timing distributions, swarm plots were generated using the Seaborn package in Python.

Cell Reports, Volume 44

Supplemental information

Rad53 regulates RNase H1, which promotes DNA replication through sites of transcription-replication conflict

Carolyn B. Wagner, Matteo Longaretti, Sophia G. Sergi, Neha Singh, Ioannis Tsirkas, Fabio Bento, Ronald P. Wong, Maya Wilkens, Stephan Hamperl, Falk Butter, Amir Aharoni, Helle D. Ulrich, and Brian Luke

Figure S1

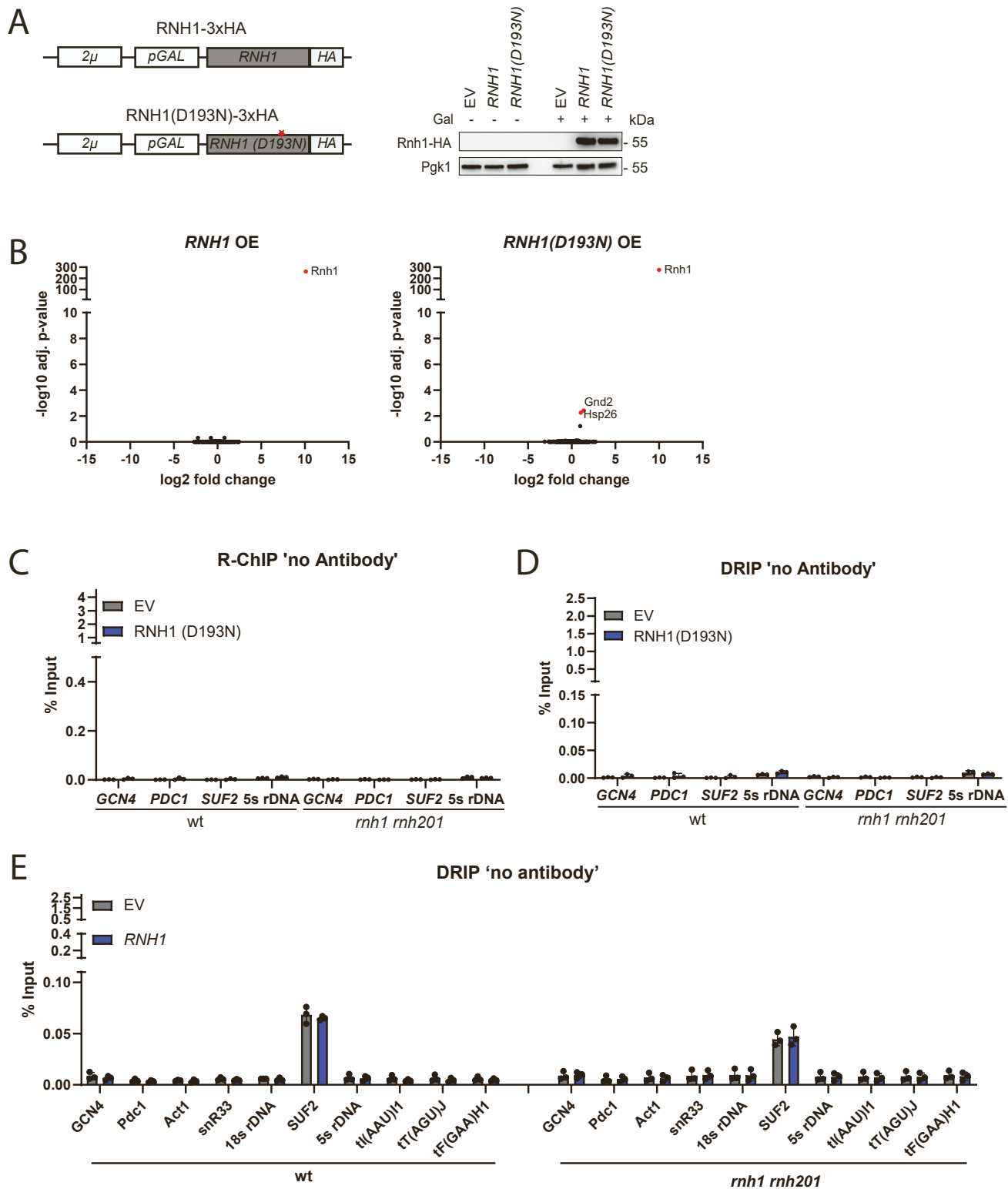


Figure S1. Overexpressed RNH1 likely acts at misregulated RNA-DNA hybrids.

(A) Left: Inducible allele for galactose induced overexpression of *RNH1*-HA and *RNH1(D193N)*-HA. Right: Confirmation of expression by Western blot analysis.

(B) Total RNA seq analysis of wild type cells overexpressing *RNH1*-HA and *RNH1(D193N)*-HA. Cells were grown to OD 0.5 in SC-Leu + 2 % raffinose prior to addition of 2 % galactose. After 2 h cells were collected for RNA extraction. Significance threshold: $p < 0.5$, $n=5$.

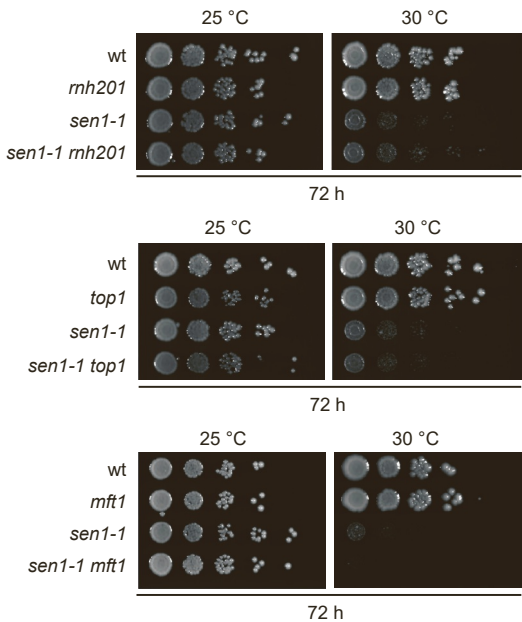
(C) No antibody control for the Rnh1(D193N) ChIP in Figure 1 C. Data are depicted as mean \pm SD, $n = 3$.

(D) No antibody control for the DRIP in Figure 1 D. Data are depicted as mean \pm SD, $n = 3$.

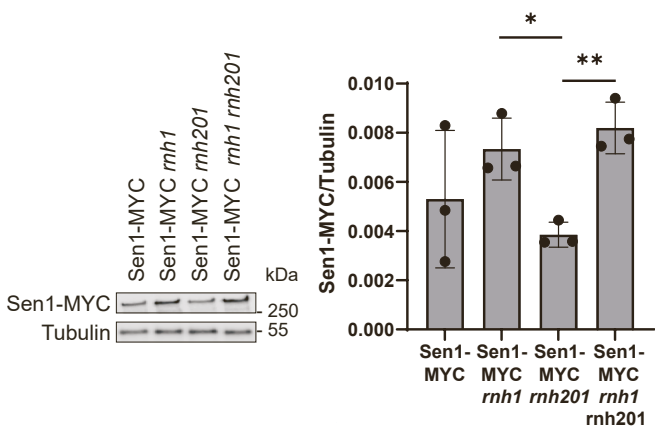
(E) No antibody control for the DRIP in Figure 1 E. Data are depicted as mean \pm SD, $n = 3$.

Figure S2

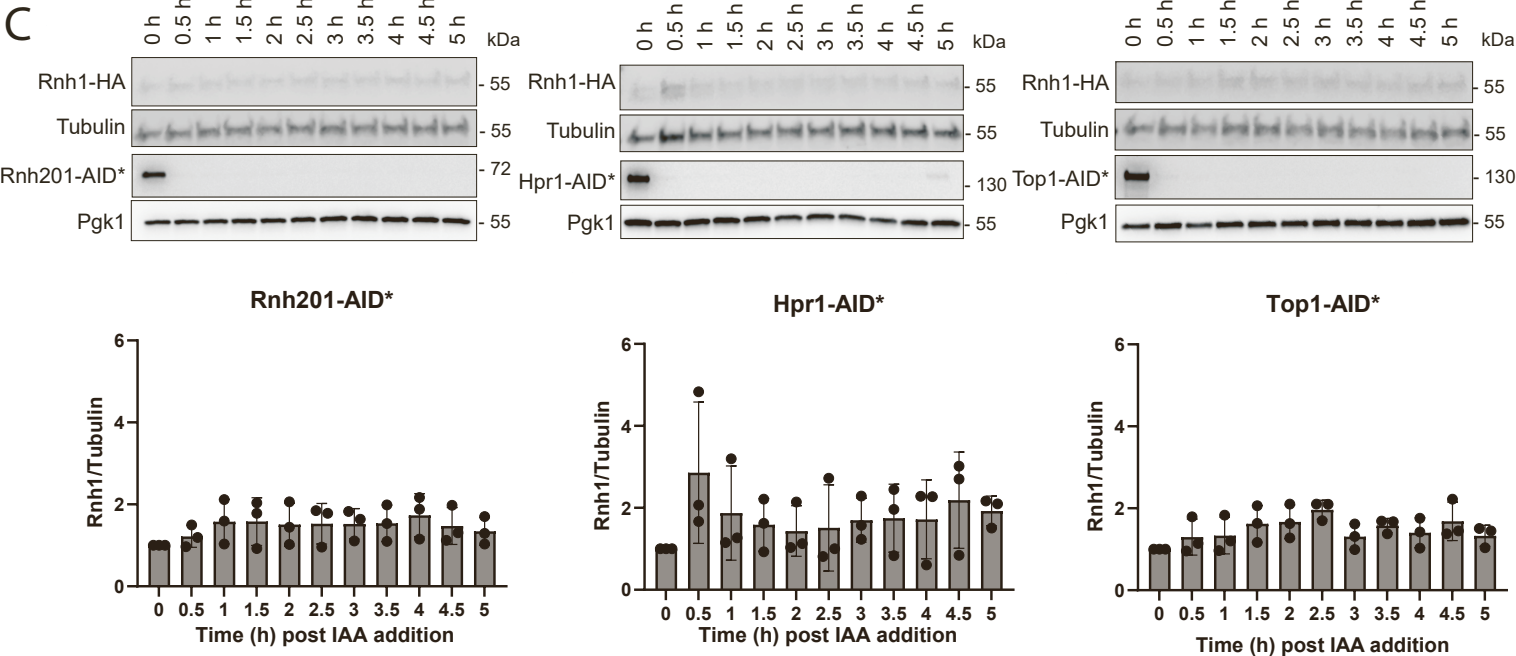
A



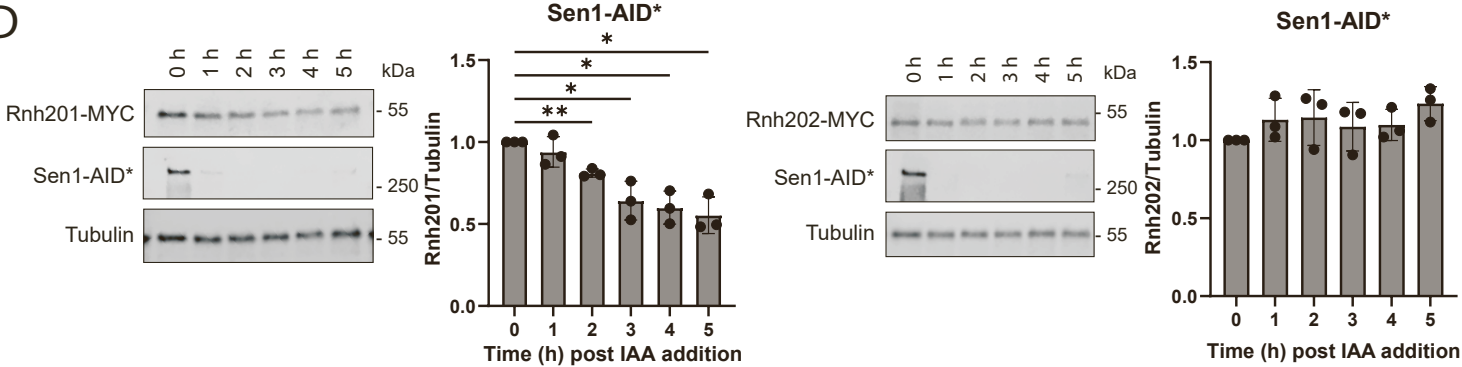
B



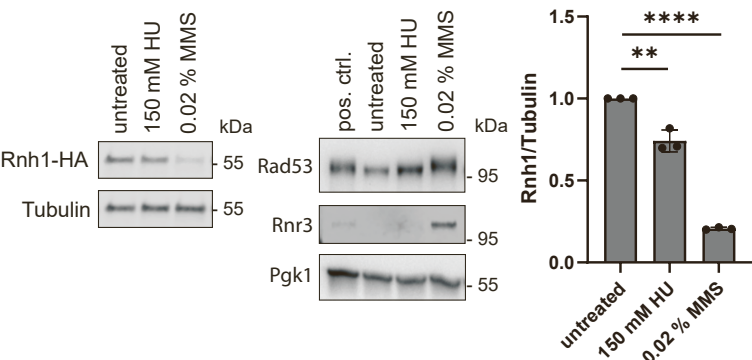
C



D



E



F

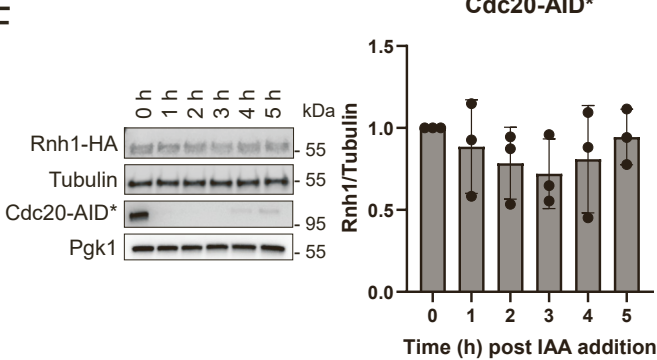


Figure S2. Increase of Rnh1 levels is specific to Sen1 loss.

- (A) Tenfold serial dilutions of the indicated strains were spotted on YPD plates and incubated at 25°C and 30 °C for 3 days.
- (B) Western blot analysis of endogenous Sen1-MYC levels in wild type and cells carrying the deletion of *RNH1*. Data are depicted as mean \pm SD, n = 3. Unpaired t-test (*: p<0.05, **: p<0.01).
- (C) Western blot analysis of endogenous Rnh1-HA levels over a time course of 5 h after depleting Rnh201-AID*, Hpr1-AID* or Top1-AID*. Values for quantification were normalized to 0 h time point. Data are depicted as mean \pm SD, n = 3.
- (D) Western blot analysis of endogenous Rnh201-MYC and Rnh202-MYC levels over a time course of 5 h after depleting Sen1-AID*. Values were normalized to the 0 h time point. Data are depicted as mean \pm SD, n = 3. Paired t-test (*: p<0.05, **: p<0.01).
- (E) Western blot analysis of endogenous Rnh1-HA levels in cells grown in the presence of 150 mM HU or 0.02 % MMS for 5 h. The positive control is a wild type sample grown in 0.02% MMS for 2 h. Values were normalized to the untreated samples. Data are depicted as mean \pm SD, n = 3. Paired t-test (**: p<0.01, ****: p<0.0001).
- (F) Western blot analysis of endogenous Rnh1-HA levels over a time course of 5 h after depleting Cdc20-AID*. Values were normalized to the 0 h time point. Data are depicted as mean \pm SD, n = 3.

Figure S3

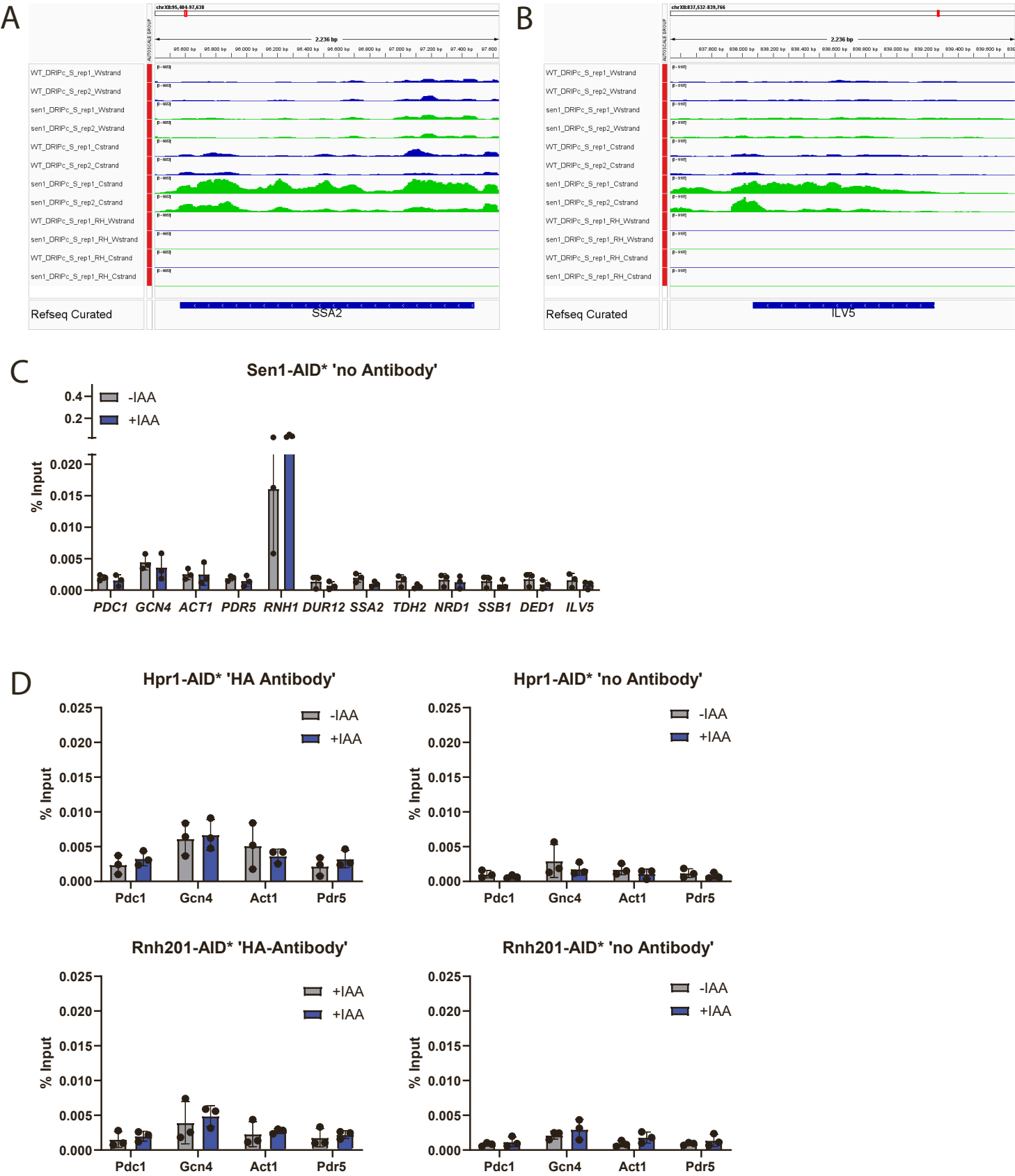
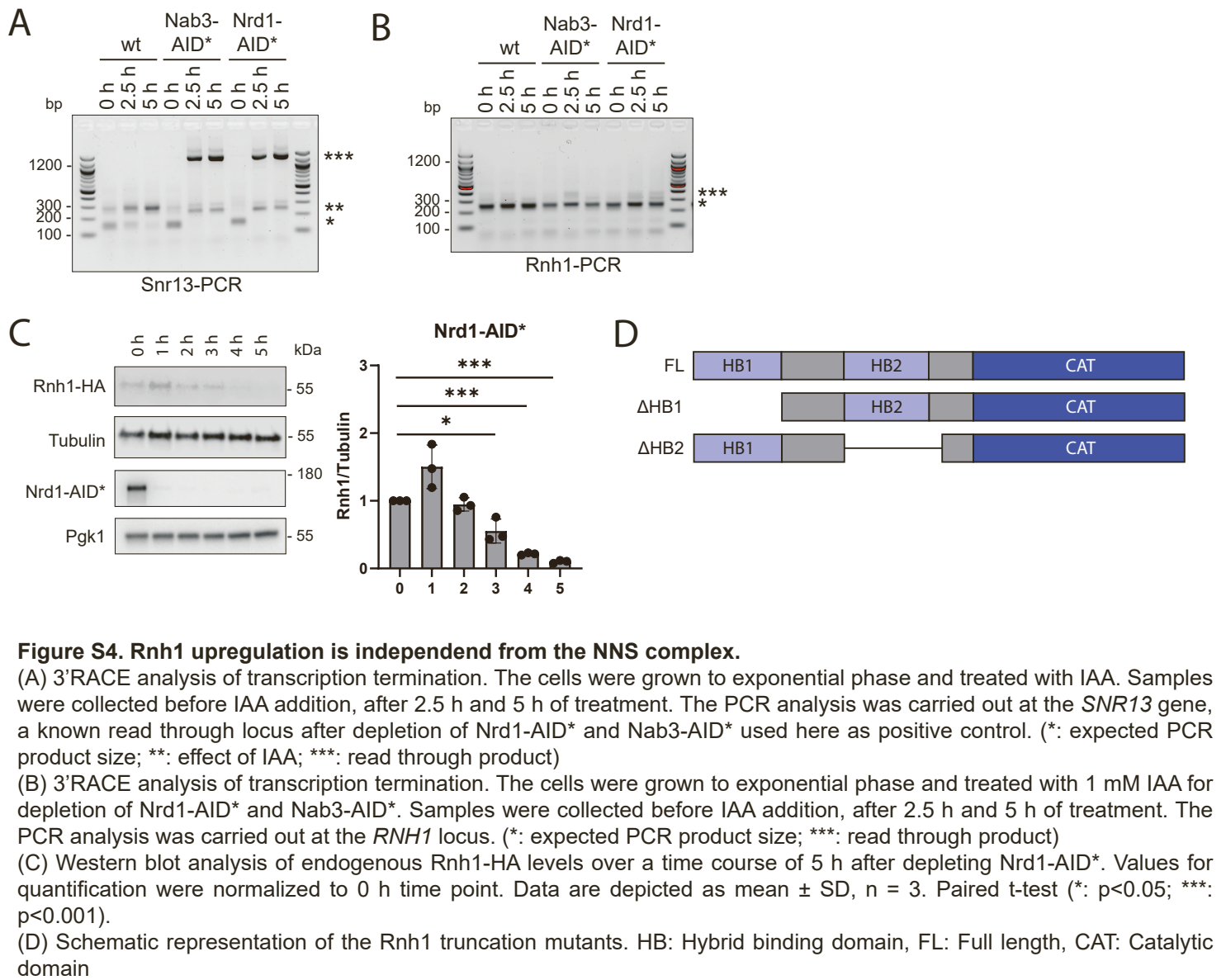


Figure S3. Rnh1 is recruited to Sen1-specific loci upon Sen1 loss.
(A) and (B) Genome Browser view of the example loci *SSA2* and *ILV5* from the DRIPc-seq experiment published in San Martin-Alonso et al (2021).
(C) No antibody control for Figure 2 F. Data are depicted as mean \pm SD, n = 3.
(D) Chromatin immunoprecipitation of endogenous catalytically inactive Rnh1-HA in a Hpr1-AID* or Rnh201-AID* background after 5 h of IAA treatment or without treatment. Left: Immunoprecipitation with HA-antibody, right: control without antibody. Data are depicted as mean \pm SD, n = 3.

Figure S4**Figure S4. Rnh1 upregulation is independent from the NNS complex.**

(A) 3'RACE analysis of transcription termination. The cells were grown to exponential phase and treated with IAA. Samples were collected before IAA addition, after 2.5 h and 5 h of treatment. The PCR analysis was carried out at the *SNR13* gene, a known read through locus after depletion of Nrd1-AID* and Nab3-AID* used here as positive control. (*: expected PCR product size; **: effect of IAA; ***: read through product)

(B) 3'RACE analysis of transcription termination. The cells were grown to exponential phase and treated with 1 mM IAA for depletion of Nrd1-AID* and Nab3-AID*. Samples were collected before IAA addition, after 2.5 h and 5 h of treatment. The PCR analysis was carried out at the *RNH1* locus. (*: expected PCR product size; ***: read through product)

(C) Western blot analysis of endogenous Rnh1-HA levels over a time course of 5 h after depleting Nrd1-AID*. Values for quantification were normalized to 0 h time point. Data are depicted as mean \pm SD, n = 3. Paired t-test (*: p<0.05; ***: p<0.001).

(D) Schematic representation of the Rnh1 truncation mutants. HB: Hybrid binding domain, FL: Full length, CAT: Catalytic domain

Figure S5

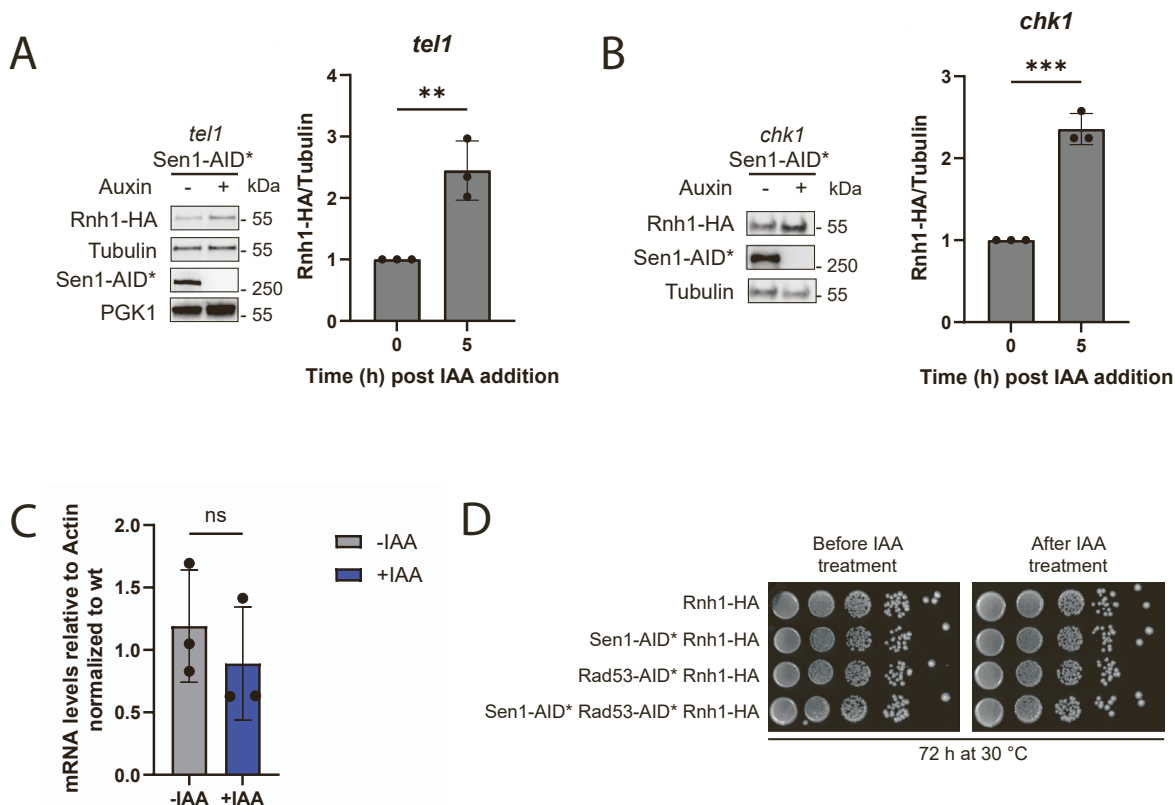


Figure S5. The replication checkpoint is required for Rnh1 accumulation

(A) Western blot analysis of endogenous Rnh1-HA levels in a *TEL1* deletion in the presence or absence of Sen1-AID* (IAA treatment for 5 h). Values were normalized to the -IAA sample. Data are depicted as mean \pm SD, n = 3. Paired t-test (**: p<0.01).

(B) Western blot analysis of endogenous Rnh1-HA levels in a *CHK1* deletion in the presence or absence of Sen1-AID* (IAA treatment for 5 h). Values were normalized to the -IAA sample. Data are depicted as mean \pm SD, n = 3. Paired t-test (*: p<0.05).

(C) Transcript levels of Rnh1 after depletion of Rad53-AID*. Cells were grown to exponential phase and treated with or without 1 mM IAA for 5 h. mRNA levels were first normalized to Actin before calculating the ratio Rad53-AID*/wild type. Data are depicted as mean \pm SD, n = 3.

(D) Impact of Rad53-AID* Sen1-AID* depletion on cell viability. Cells were grown to exponential phase and treated with or without 1 mM IAA for 5 h. The cells were washed thrice in sterile ddH₂O. A tenfold serial dilution of these samples was spotted on YPD plates and incubated at 30 °C for 3 days.

Figure S6

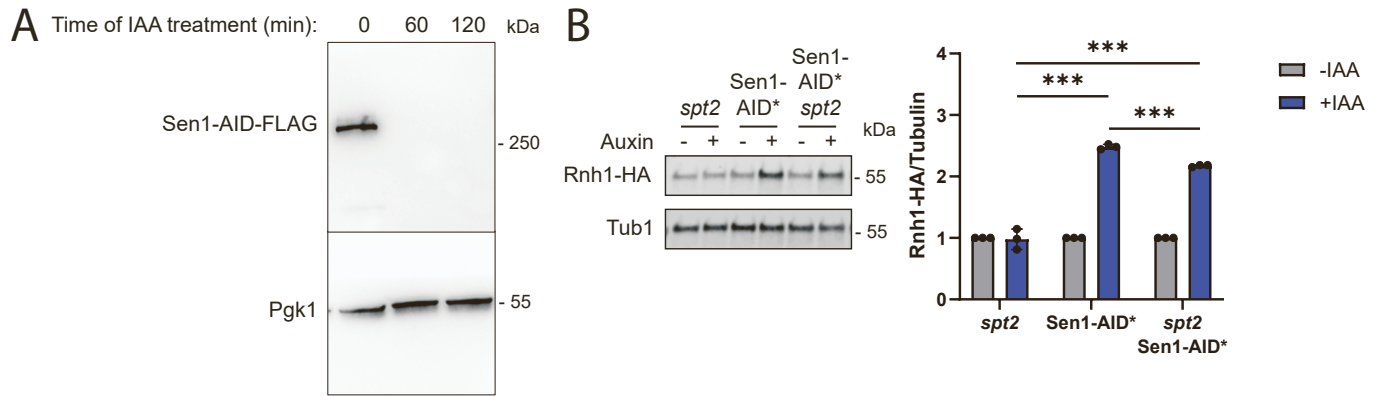


Figure S6. Rnh1 assists with timely replication completion through TRCs.

(A) Western blot confirming the depletion of Sen1-AID-FLAG in the microscopy assay performed in Figure 5D.

(B) Western blot analysis of endogenous Rnh1-HA levels in a *SPT2* deletion in the presence or absence of Sen1-AID* (IAA treatment for 5 h). Values were normalized to the -IAA samples. Data are depicted as mean \pm SD, n = 3. Unpaired t-test (***: p<0.001).

Table S1. Yeast Strains used in this study

Strain name	Genotype	Source
yAL637	MATa his3Δ1 leu2Δ0 ura3Δ0 met15Δ0 sen1-1::KAN rnh201::HYG	This study
yCW3, 4 and 5	MATa his3Δ1 leu2Δ0 ura3Δ0 met15Δ0	This study
yCW13, 19, 25	MATa his3Δ1 leu2Δ0 ura3Δ0 met15Δ0 + pBL211	This study
yCW15, 21, 27	MATa his3Δ1 leu2Δ0 ura3Δ0 met15Δ0 + pBL352	This study
yCW17, 23, 28	MATa his3Δ1 leu2Δ0 ura3Δ0 met15Δ0 + pBL633	This study
yCW70, 71, 244 and 250	MATa his3Δ1 leu2Δ0 ura3Δ0 met15Δ0 sen1-1::kan + pBL211	This study
yCW72, 73, 246 and 252	MATa his3Δ1 leu2Δ0 ura3Δ0 met15Δ0 sen1-1::kan + pBL352	This study
yCW74, 75, 248 and 254	MATa his3Δ1 leu2Δ0 ura3Δ0 met15Δ0 sen1-1::kan + pBL633	This study
yCW78, 79 and 80	MATalpha his3Δ1 leu2Δ0 ura3Δ0 lys2Δ0 rad52::kan + pBL211	This study
yCW340, 341 and 342	MATa his3Δ1 leu2Δ0 ura3Δ0 met15Δ0 LYS2 rnh1::kan	This study
yCW347, 348 and 349	MATa his3Δ1 leu2Δ0 ura3Δ0 met15Δ0 LYS2 rnh201::hyg	This study
yCW354, 355 and 356	MATa his3Δ1 leu2Δ0 ura3Δ0 met15Δ0 LYS2 rnh1::kan rnh201::hyg	This study
yCW372, 373	his3Δ1 leu2Δ0 ura3Δ0 met15Δ0 rnh1::kan rnh201::hyg + pBL211	This study
yCW374, 375	his3Δ1 leu2Δ0 ura3Δ0 met15Δ0 rnh1::kan rnh201::hyg + pBL352	This study
yCW376, 377	his3Δ1 leu2Δ0 ura3Δ0 met15Δ0 rnh1::kan rnh201::hyg + pBL633	This study
yCW540, 541 and 542	MATa his3Δ1 LEU2::AFB2-LEU2 met15Δ0 ura3Δ0 RNH1-6xHA::KAN Rnh201-AID*-9Myc-His	This study
yCW545, 546 and 547	MATa his3Δ1 LEU2::AFB2-LEU2 met15Δ0 ura3Δ0 RNH1-6xHA::KAN Sen1-AID*-9Myc-His	This study
yCW550, 551 and 552	MATa his3Δ1 LEU2::AFB2-LEU2 ura3Δ0 RNH1-6xHA::KAN Top1-AID*-9Myc-His	This study
yCW694 and 695	MATalpha his3Δ1 leu2Δ0 met15Δ0 ura3Δ0 Hpr1-AID*-9Myc-His Trp1::GDP-OsTIR1(F74G)-Nat RNH1-6xHA::KAN	This study
yCW696	MATa his3Δ1 leu2Δ0 met15Δ0 ura3Δ0 Hpr1-AID*-9Myc-His Trp1::GDP-OsTIR1(F74G)-Nat RNH1-6xHA::KAN	This study
yCW730, 731 and 732	MATa his3Δ1 leu2Δ0 met15Δ0 ura3Δ0 met15Δ0 LYS2 top1::HYG + pBL211	This study
yCW733, 734 and 735	MATa his3Δ1 leu2Δ0 met15Δ0 ura3Δ0 met15Δ0 LYS2 top1::HYG + pBL352	This study
yCW736, 737 and 738	MATa his3Δ1 leu2Δ0 met15Δ0 ura3Δ0 met15Δ0 LYS2 top1::HYG + pBL633	This study
yCW828	MATalpha his3Δ1 leu2Δ0 ura3Δ0 met15Δ0 Can1 lyp1Δ::GPD-OsTIR1(F74G)-NAT Nab3-AID*-9xMYC::Hyg	This study
yCW829	MATa his3Δ1 leu2Δ0 ura3Δ0 met15Δ0 Can1 lyp1Δ::GPD-OsTIR1(F74G)-NAT Nab3-AID*-9xMYC::Hyg	This study
yCW831, 832 and 833	MATa his3Δ1 leu2Δ0 ura3Δ0 met15Δ0 Can1 lyp1Δ::GPD-OsTIR1(F74G)-NAT Nab3-AID*-9xMYC::Hyg Rnh1-HA (Kan)	This study
yCW834	MATalpha his3Δ1 leu2Δ0 ura3Δ0 met15Δ0 Can1 lyp1Δ::GPD-OsTIR1(F74G)-NAT Nrd1-AID*-9xMYC::Hyg	This study
yCW835	MATa his3Δ1 leu2Δ0 ura3Δ0 met15Δ0 Can1 lyp1Δ::GPD-OsTIR1(F74G)-NAT Nrd1-AID*-9xMYC::Hyg	This study
yCW837 and 838	MATalpha his3Δ1 leu2Δ0 ura3Δ0 met15Δ0 Can1 lyp1Δ::GPD-OsTIR1(F74G)-NAT Nrd1-AID*-9xMYC::Hyg Rnh1-HA (Kan)	This study
yCW839	MATa his3Δ1 leu2Δ0 ura3Δ0 met15Δ0 Can1 lyp1Δ::GPD-OsTIR1(F74G)-NAT Nrd1-AID*-9xMYC::Hyg Rnh1-HA (Kan)	This study
yCW919, 920 and 921	MATa his3Δ1 leu2Δ0 ura3Δ0 rnh1::hyg	This study
yCW922, 923 and 924	MATa his3Δ1 leu2Δ0 ura3Δ0 sen1-1::Kan	This study
yCW925, 926 and 927	MATa his3Δ1 leu2Δ0 ura3Δ0 rnh1::Hyg sen1-1::Kan	This study

yCW929, 930 and 931	MATa his3Δ1 leu2Δ0 met15Δ0 ura3Δ0 mft1::Kan + pBL211	This study
yCW932, 933 and 934	MATa his3Δ1 leu2Δ0 met15Δ0 ura3Δ0 mft1::Kan + pBL352	This study
yCW935, 936 and 937	MATa his3Δ1 leu2Δ0 met15Δ0 ura3Δ0 mft1::Kan + pBL633	This study
yCW967, 968 and 969	MATa his3Δ1 LEU2::AFB2-LEU2 ura3Δ0 RNH201-6MYC-URA sen1::AID-HIS	This study
yCW971, 972 and 973	MATa his3Δ1 LEU2::AFB2-LEU2 ura3Δ0 RNH202-3MYC-URA sen1::AID-HIS	This study
yCW977, 978 and 979	MATalpha his3Δ1 leu2Δ0 met15Δ0 ura3Δ0 Trp1::GDP-OsTIR1(F74G)-Nat RNH1-6xHA::KAN Sen1-AID*-9Myc-His + pBL211	This study
yCW980, 981 and 982	MATalpha his3Δ1 leu2Δ0 met15Δ0 ura3Δ0 Trp1::GDP-OsTIR1(F74G)-Nat RNH1-6xHA::KAN Sen1-AID*-9Myc-His + pBL1117	This study
yCW1013, 1014, 1015	MATa his3Δ1 leu2Δ0 ura3Δ0 met15Δ0 top1::HYG	This study
yCW1019, 1020, 1021	MATa his3Δ1 leu2Δ0 ura3Δ0 met15Δ0 top1::HYG sen1-1::Kan	This study
yCW1049, 1050 and 1051	MATa his3Δ1 leu2Δ0 met15Δ0 ura3Δ0 mft1::Hyg rnh1::Kan	This study
yCW1052, 1053 and 1054	MATa his3Δ1 leu2Δ0 met15Δ0 ura3Δ0 mft1::Hyg	This study
yCW1061, 1062 and 1063	MATa his3Δ1 GPD-AFB2 (Leu) ura3Δ0 RNH1-6xHA::KAN Sen1-AID*-9Myc-His bar1::Nat	This study
yCW1069, 1070 and 1071	MATa his3Δ1 leu2Δ0 ura3Δ0 met15Δ0 rnh1::kan top1::HYG	This study
yCW1380, 1381 and 1382	MATa his3Δ1 GPD-AFB2 (Leu) ura3Δ0 Rnh1(D913N)-6xHA::KAN Sen1::AID-HIS	This study
yCW1384, 1385 and 1386	MATa his3Δ1 GPD-AFB2 (Leu) ura3Δ0 Rnh1(D913N)-6xHA::KAN Rnh201::AID-HIS	This study
yCW1429, 1430 and 1431	MATa his3Δ1 leu2Δ ura3Δ0 Rnh1(D913N)-6xHA::KAN Hpr1-AID*-9Myc-His Trp1::GDP-OsTIR1(F74G)-Nat	This study
yCW1433, 1434 and 1435	MATa his3Δ1 leu2Δ0 ura3Δ0 met15Δ0 LYS2 sen1-1::Hyg mft1::Kan	This study
yCW1506	MATa his3Δ1 leu2Δ0 ura3Δ0 Sen1-AID-Myc (His) pGpd-AFB2 (Leu)	This study
yCW1509	MATa his3Δ1 leu2Δ0 ura3Δ0 Sen1-AID-Myc (His) pGpd-AFB2 (Leu) rnh1::KAN	This study
yCW1603, 1604 and 1605	MATa his3Δ1 leu2Δ0 ura3Δ0 met15Δ0 LYS2 + pBL211 (EV)	This study
yCW1609, 1610 and 1611	MATalpha his3Δ1 leu2Δ0 ura3Δ0 met15Δ0 rnh1::HIS + pBL211 (EV)	This study
yCW1615, 1616 and 1617	MATa his3Δ1 leu2Δ0 ura3Δ0 Trp1::GDP-OsTIR1(F74G)-Nat Sen1-AID*-9MYC (HIS) rnh1::Kan + pBL211 (EV)	This study
yCW1618, 1619 and 1620	MATa his3Δ1 leu2Δ0 ura3Δ0 Trp1::GDP-OsTIR1(F74G)-Nat Sen1-AID*-9MYC (HIS) rnh1::Kan + pBL352 (RNH1 OE)	This study
yCW1621, 1622 and 1623	MATa his3Δ1 leu2Δ0 ura3Δ0 Trp1::GDP-OsTIR1(F74G)-Nat Sen1-AID*-9MYC (HIS) + pBL211 (EV)	This study
yFB130	MATa his3Δ1 leu2Δ0 ura3Δ0 met15Δ0 lys2Δ0	This study
yFB405 and 406	MATa his3Δ1 leu2Δ0 ura3Δ0 sen1-1::KAN rnh201::NAT	This study
yFB1175	MATa his3Δ1 leu2Δ0 met15Δ0 ura3Δ0 rnh1::KAN rnh201::HYG + pBL906	This study
yFB1355 and 1356	MAT a his3Δ1 leu2Δ0 met15Δ0 ura3Δ0 rnh1::KAN rnh201::HYG + pBL797	This study
yFB1364	MATa his3Δ1 leu2Δ0 met15Δ0 ura3Δ0 rnh1::KAN rnh201::HYG + pBL804	This study
yFB1367	MATa his3Δ1 leu2Δ0 met15Δ0 ura3Δ0 rnh1::KAN rnh201::HYG + pBL808	This study
yFB1424 and 1425	MATa his3Δ1 leu2Δ0 met15Δ0 ura3Δ0 + pBL906	This study
yFB1426 and 1427	MAT a his3Δ1 leu2Δ0 met15Δ0 ura3Δ0 + pBL797	This study
yFB1428 and 1429	MAT a his3Δ1 leu2Δ0 met15Δ0 ura3Δ0 + pBL837	This study

yFB1492 and 1493	MAT a his3Δ1 leu2Δ0 met15Δ0 ura3Δ0 rnh1::KAN rnh201::HYG + pBL837	This study
yFB1541 and 1542	MAT a his3Δ1 leu2Δ0 met15Δ0 ura3Δ0 rnh1::KAN rnh201::HYG + pBL906	This study
yFB2426	MATa his3Δ1 leu2Δ0 ura3Δ0 met15Δ0 RNH1-6xHA::KAN Sen1::AID-HIS GPD-AFB2::LEU	This study
yFB2427	MATalpha his3Δ1 leu2Δ0 ura3Δ0 met15Δ0 RNH1-6xHA::KAN Sen1::AID-HIS GPD-AFB2::LEU	This study
yFB2433	MATalphahis3Δ1 leu2Δ0 ura3Δ0 met15Δ0 RNH1-ΔHB1-6xHA::KAN Sen1::AID-HIS GPD-AFB2::LEU	This study
yFB2434	MATa his3Δ1 leu2Δ0 ura3Δ0 met15Δ0 RNH1-ΔHB1-6xHA::KAN Sen1::AID-HIS GPD-AFB2::LEU	This study
yFB2450	MATahis3Δ1 leu2Δ0 ura3Δ0 met15Δ0 RNH1-ΔHB2-6xHA::KAN Sen1::AID-HIS GPD-AFB2::LEU	This study
yFB2451	MATalphahis3Δ1 leu2Δ0 ura3Δ0 met15Δ0 RNH1-ΔHB2-6xHA::KAN Sen1::AID-HIS GPD-AFB2::LEU	This study
yML69, 70, 71	MATa his3Δ1 leu2Δ ura3Δ0 RNH1-6xHA::KAN	This study
yML73, 74, 75	MATa his3Δ1 leu2Δ0 ura3Δ0 SEN1-AID-MYC-HIS GPD-AFB2 (LEU) RNH1-6xHA::KAN	This study
yML101, 102, 103	MATa his3Δ1 leu2Δ0 ura3Δ0 SEN1-AID-MYC-HIS GPD-AFB2 (LEU) RNH1-6xHA::KAN chk1::HYG	This study
yML113, 114, 115	MATa his3Δ1 leu2Δ0 ura3Δ RNH1-6xHA::KAN RAD53-AID*-9MYC-HYG GDP AFB2 (LEU)	This study
yML117, 118, 119	MATa his3Δ1 leu2Δ0 ura3Δ RNH1-6xHA::KAN RAD53-AID*-9MYC-HYG GDP AFB2 (LEU) sen1::AID-MYC-HIS	This study
yML77, 78, 79	MATa his3Δ1 leu2Δ0 ura3Δ0 SEN1-AID-MYC-HIS GPD-AFB2 (LEU) RNH1-6xHA::KAN rad9::NAT	This study
yML93, 94, 95	MATa his3Δ1 leu2Δ0 ura3Δ0 SEN1-AID-MYC-HIS GPD-AFB2 (LEU) RNH1-6xHA::KAN mrc1::HYG	This study
yML169, 107, 171	MATa his3Δ1 leu2Δ0 ura3Δ0 SEN1-AID-MYC-HIS GPD-AFB2 (LEU) RNH1-6xHA::KAN rad9::NAT Mrc1-AID*::URA	This study
yML85, 86, 87	MATa his3Δ1 leu2Δ0 ura3Δ0 SEN1-AID-MYC-HIS GPD-AFB2 (LEU) RNH1-6xHA::KAN tel1::HYG	This study
yML199,201	MATalpha his3Δ1leu2Δ0 ura3Δ0 Sen1-MYC-His	This study
yML203,205	MATalpha his3Δ1leu2Δ0 ura3Δ0 rnh1::KAN Sen1-MYC::His	This study
yOV91	MATs his3Δ1 LEU2::AFB2-LEU2 met15Δ0 ura3Δ0 Rad53-AID-Myc (Hyg)	This study
ySGS20, 21	MATa his3Δ1 leu2Δ0 met15Δ0 ura3Δ0 LYS2 RNH1-6xHA (KAN) sen1-3-9xMyc (His) rnh201::NAT	This study
ySGS22	MATalpha his3Δ1 leu2Δ0 met15Δ0 ura3Δ0 LYS2 RNH1-6xHA (KAN) sen1-3-9xMyc (His) rnh201::NAT	This study
ySGS23, 24	MATalpha his3Δ1 leu2Δ0 met15Δ0 ura3Δ0 LYS2 RNH1-6xHA (KAN) sen1-3-9xMyc (His)	This study
ySGS25	MATa his3Δ1 leu2Δ0 met15Δ0 ura3Δ0 LYS2 RNH1-6xHA (KAN) sen1-3-9xMyc (His)	This study
ySGS26, 27	MATa his3Δ1 leu2Δ0 met15Δ0 ura3Δ0 LYS2 RNH1-6xHA (KAN) rnh201::NAT	This study
ySGS28	MATalpha his3Δ1 leu2Δ0 met15Δ0 ura3Δ0 LYS2 RNH1-6xHA (KAN) rnh201::NAT	This study
ySGS29	MATalpha his3Δ1 leu2Δ0 met15Δ0 ura3Δ0 LYS2 RNH1-6xHA (KAN)	This study
ySGS30, 31	MATa his3Δ1 leu2Δ0 met15Δ0 ura3Δ0 LYS2 RNH1-6xHA (KAN)	This study

Table S2: Oligonucleotides used in this study

Name	Sequence	Target gene	Direction	Application	Source
oAL8	GGACACGATGGTGATCCA GG	Rnh1	Forward	Confirmation of C-terminal AID tag, 3'RACE	
oAL31	ATGGACAGCAGGAAGAA CG	Rnh201	Forward	3'RACE	
oAL76	ccttgatacgagcgtaacctca	Pdc1	Forward	qPCR	
oAL78	gaaggatgagatgggctggtaa	Pdc1	Reverse	qPCR	
oBL292	CCCAGGTATTGCCGAAAG AATGC	Actin	Forward	ddPCR; qPCR	
oBL293	TTTGTTGGAAGGTAGTCA AAGAAGCC	Actin	Reverse	ddPCR; qPCR	
oCW68	TACGCGGTTAGAAAGGGC AG	Rnh1	Forward	ddPCR	
oCW69	CCAGCATGCGTTGAACTT CC	Rnh1	Reverse	ddPCR	
oCW118	AGTTCACCGACGAGAA AC	Rnh201	Forward	ddPCR	
oCW119	ATGCAGTAGAGCGAGTCT GC	Rnh201	Reverse	ddPCR	
oCW120	CACTTTTACACTGCCGCCA C	Rnh202	Forward	ddPCR	
oCW121	GGCCCTTGCCGAATTGA AA	Rnh202	Reverse	ddPCR	
oCW122	GCCATCCTCTCGGGAAC AC	Rnh203	Forward	ddPCR	
oCW123	CGCCAATTCGTTGCGATC AG	Rnh203	Reverse	ddPCR	
oCW128	TTCGTATACCCGGGTACC AATTTTTTTTTTTTTTTT	Poly-A	Reverse	3'RACE RT	Mischo et al., 2011
oCW129	TTGGTACCCGGGTATACG AA	3'RACE adaptor	Reverse	3'RACE adaptor primer	Mischo et al., 2012
oCW130	GTGGTGACACTGCCACTG TC	Pgk1	Forward	3'RACE	
oCW137	GTGCCATGAATGTAGGCC TAAATTC	Rnh202	Forward	3'RACE	
oCW139	CGAATTGGCGCGATTGCA AG	Rnh203	Forward	3'RACE	
oCW140	GATGAATATGAGTGCATT TGGCTCG	Snr13	Forward	3'RACE	
oCW157	GATGGACGTAGTGAGTGC ATTTGTAGACC	Sen1	Forward	sen1-3 HR template for CRISPR, confirmation of sen1-3	

oCW179	TTTGGTCTCACGCATAAA ATTCTGGGAATCATGTGT TTTAGAGCTAGAAATAGC AAGTTA	pBL1158	Forward	Golden Gate assembly (Bsal) of pBL1168	
oCW180	TTTGGTCTCAGGATTGCG CAAGCCGGAATCG	pBL1158	Reverse	Golden Gate assembly (Bsal) of pBL1168	
oCW181	aaacaactgtgtgaccttgag	pBL1168	Forward	confirmation of pBL1168	
oCW182	acacatgtatctcagatatctcatt atatc	pBL1168	Reverse	confirmation of pBL1168	
oCW183	CACCAAAGAGCGACTTAG ATCTAAAG	Sen1	Reverse	sen1-3 HR template for CRISPR, confirmation of sen1-3	
oCW184	GTCAGAGGCTATATTTCA CTGGAGAA	Pdr5	Forward	qPCR	(San Martin-Alonso <i>et al.</i> , 2021)
oCW185	TACGTCTTGTTTCGGCCTT AATC	Pdr5	Reverse	qPCR	(San Martin-Alonso <i>et al.</i> , 2021)
oFB346	AGCTGATGATTGGAACGT ACC	Sen1	Reverse	confirmation of sen1-3	
oFB349	CTGGACAGAGATTGTGGT ATCTC	Sen1	Forward	confirmation of sen1-3	
oLP178	TTGTGCCCGAATCC AGTGA	Gcn4	Forward	qPCR	(Santos-Pereira <i>et al.</i> , 2013; San Martin-Alonso <i>et al.</i> , 2021)
oLP179	TGGCGGCTTCAGTG TTTCTA	Gcn4	Reverse	qPCR	(Santos-Pereira <i>et al.</i> , 2013; San Martin-Alonso <i>et al.</i> , 2021)

Table S3: Plasmids used in this study

Plasmid identifier	Plasmid name	Source
pBL211	pRS425 pGal	Gift from M. Peter
pBL352	pRS425 pGal-RNH1-HA	Graf et al., 2017
pBL633	pRS425 pGal-RNH1(D193N)-HA	Wagner and Luke, 2022
pBL797	pRS416 pGal-RNH1-HA	This study
pBL804	pGal-RNH1(D193N)-HA delta52	This study
pBL808	pGal-RNH1(D193N)-HA delta53-168	This study
pBL837	pRS416 pGal-RNH1(D193N)-HA	Misino et al., 2022
pBL906	pRS416 pGal-3HA	Misino et al., 2022
pBL959	pRS426-Gal-EV-3HA	This study
pBL967	pRS426-Gal-RNH1(D193N)-3HA	This study
pBL1117	pRS425 pGal-RNH1-3Myc	This study
pBL1158	pMYT095 CRISPR/Cas9-gRNA empty backbone	Addgene
pBL1168	CRISPR/Cas9-Sen1-gRNA	This study